SAND99-2021J

Direct Releases to the Surface and Associated Complementary Cumulative Distribution Functions in the 1996 Performance Assessment for the Waste Isolation Pilot Plant: Direct Brine Release

D.M. Stoelzel[a], D.G. O'Brien[b], J.W. Garner[c], J.C. Helton[d], J.D. Johnson[e], and L.N. Smith[f]

[a]Sandia National Laboratories, Albuquerque, NM 87185 USA; [b]Solutions Engineering, Lakewood, CO 80232 USA; [c]Piru Associates, Albuquerque, NM 87106 USA; [d]Department of Mathematics, Arizona State University, Tempe, AZ 85287 USA; [e]GRAM, Inc., Albuquerque, NM 87112 USA; [f]Comforce, Albuquerque, NM 87110 USA

Abstract

The following topics related to the treatment of direct brine releases to the surface environment in the 1996 performance assessment for the Waste Isolation Pilot Plant (WIPP) are presented: (i) mathematical description of models, (ii) uncertainty and sensitivity analysis results arising from subjective (i.e., epistemic) uncertainty for individual releases, (iii) construction of complementary cumulative distribution functions (CCDFs) arising from stochastic (i.e., aleatory) uncertainty, and (iv) uncertainty and sensitivity analysis results for CCDFs. The presented analyses indicate that direct brine releases do not constitute a serious threat to the effectiveness of the WIPP as a disposal facility for transuranic waste. Even when the effects of uncertain analysis inputs are taken into account, the CCDFs for direct brine releases fall substantially to the left of the boundary line specified in the U.S. Environmental Protection Agency's standard for the geologic disposal of radioactive waste (40 CFR 191, 40 CFR 194).

Key Words: Aleatory uncertainty, compliance certification application, direct brine release, epistemic uncertainty, Latin hypercube sampling, Monte Carlo, performance assessment, radioactive waste, risk, stochastic uncertainty, subjective uncertainty, transuranic waste, Waste Isolation Pilot Plant, 40 CFR 191, 40 CFR 194.

Please send page proof to:

Jon C. Helton
Department 6848, MS 0779
Sandia National Laboratories
Albuquerque, NM 87185-0779, USA
Phone: 505-284-4808
Fax: 505-844-2348
email: jchelto@sandia.gov

DISCLAIMER

DISCLAIMER

Portions of this document may be illegible in electronic image products. Images are produced from the best available original document.

1. Introduction

The Waste Isolation Pilot Plant (WIPP) is under development by the U.S. Department of Energy (DOE) for the geologic disposal of transuranic waste. This article describes the modeling of direct brine releases (DBRs) to the surface (i.e., the accessible environment) at the time of an inadvertent drilling intrusion into the waste panels associated with the WIPP and the construction of associated complementary cumulative distribution functions (CCDFs) for comparison with U.S. Environmental Protection Agency's (EPA's) standard for the geologic disposal of radioactive waste.[1-4] The presented DBR model and associated results constitute part of the 1996 performance assessment (PA) for the WIPP and support a compliance certification application (CCA) by the DOE to the EPA for the certification of the WIPP for the disposal of transuranic waste.[5]

In the 1996 WIPP PA, DBR refers to releases of radionuclides to the surface due to the rapid flow of radionuclide-contaminated brine into the borehole and then to the surface at the time that a drilling intrusion penetrates the repository. The release itself is then given by the product of the amount of brine that reaches the surface and the radionuclide concentration in that brine. Such releases have the potential to occur when the pressure in the repository at the time of a drilling intrusion exceeds 8 MPa, which is the pressure exerted by a column of brine-saturated drilling fluid at the depth of the repository.[6] For repository pressures less than 8 MPa, no DBRs are assumed to occur. However, even if the repository pressure exceeds 8 MPa at the time of a drilling intrusion, a DBR is not assured as there may not be sufficient mobile brine in the repository to result in brine movement to the intruding borehole.

At a conceptual level, the 1996 PA for the WIPP is underlain by three entities (EN1, EN2, EN3): EN1, a probabilistic characterization of the likelihood of different futures occurring at the WIPP site over the next 10,000 yr (Sect. 3, Ref. 7); EN2, a procedure for estimating the radionuclide releases to the accessible environment associated with each of the possible futures that could occur at the WIPP site over the next 10,000 yr (Sect. 4, Ref. 7); and EN3, a probabilistic characterization of the uncertainty in the parameters used in the definitions of EN1 and EN2 (Sect. 5, Ref. 7). All three of these entities play a role in the DBR results presented in this article. In particular, the following topics are considered: (i) models used to estimate DBRs, which constitute part of EN2 (Sect. 4, Ref. 7); (ii) construction of CCDFs for DBRs, which involves the probability space for stochastic uncertainty associated with EN1 (Sect. 3, Ref. 7; Ref. 8); and (iii) uncertainty and sensitivity analysis to assess the implications of uncertain analysis inputs, which involves the probability space for subjective uncertainty associated with EN3 (Sect. 5, Ref. 7; Ref. 9).

When viewed formally, EN2 is defined by a function f of the form

$$f(\mathbf{x}_{st}) = f_C(\mathbf{x}_{st}) + f_{SP}\left[\mathbf{x}_{st}, f_B(\mathbf{x}_{st})\right] + f_{DBR}\left\{\mathbf{x}_{st}, f_{SP}\left[\mathbf{x}_{st}, f_B(\mathbf{x}_{st})\right], f_B(\mathbf{x}_{st})\right\}$$

$$+ f_{MB}\left[\mathbf{x}_{st}, f_B(\mathbf{x}_{st})\right] + f_{DL}\left[\mathbf{x}_{st}, f_B(\mathbf{x}_{st})\right] + f_S\left[\mathbf{x}_{st}, f_B(\mathbf{x}_{st})\right]$$

$$+ f_{S-T}\left\{\mathbf{x}_{st,0}, f_{S-F}(\mathbf{x}_{st,0}), f_{N-P}\left[\mathbf{x}_{st}, f_B(\mathbf{x}_{st})\right]\right\}, \quad (1)$$

where $\mathbf{x}_{st}$ ~ particular future under consideration, $\mathbf{x}_{st,0}$ ~ future involving no drilling intrusions but a mining event at the same time t_{min} as in $\mathbf{x}_{st}$, $f_C(\mathbf{x}_{st})$ ~ cuttings and cavings release to accessible environment for $\mathbf{x}_{st}$ calculated with CUTTINGS_S, $f_B(\mathbf{x}_{st})$ ~ two-phase flow results calculated for $\mathbf{x}_{st}$ with BRAGFLO (in practice, $f_B(\mathbf{x}_{st})$ is a vector containing a large amount of information), $f_{SP}\left[\mathbf{x}_{st}, f_B(\mathbf{x}_{st})\right]$ ~ spallings release to accessible environment for $\mathbf{x}_{st}$ calculated with the spallings model contained in CUTTINGS_S; this calculation requires BRAGFLO results (i.e., $f_B(\mathbf{x}_{st})$) as input, $f_{DBR}\left\{\mathbf{x}_{st}, f_{SP}\left[\mathbf{x}_{st}, f_B(\mathbf{x}_{st})\right], f_B(\mathbf{x}_{st})\right\}$ ~ direct brine release to accessible environment for $\mathbf{x}_{st}$ calculated with a modified version of BRAGFLO designated BRAGFLO_DBR; this calculation requires spallings results obtained from CUTTINGS_S (i.e., $f_{SP}[\mathbf{x}_{st}, f_B(\mathbf{x}_{st})]$) and BRAGFLO results (i.e., $f_B(\mathbf{x}_{st})$) as input, $f_{MB}\left[\mathbf{x}_{st}, f_B(\mathbf{x}_{st})\right]$ ~ release through anhydrite marker beds to accessible environment for $\mathbf{x}_{st}$ calculated with NUTS; this calculation requires BRAGFLO results (i.e., $f_B(\mathbf{x}_{st})$) as input, $f_{DL}\left[\mathbf{x}_{st}, f_B(\mathbf{x}_{st})\right]$ ~ release through Dewey Lake Red Beds to accessible environment for $\mathbf{x}_{st}$ calculated with NUTS; this calculation requires BRAGFLO results (i.e., $f_B(\mathbf{x}_{st})$) as input, $f_S\left[\mathbf{x}_{st}, f_B(\mathbf{x}_{st})\right]$ ~ release to land surface due to brine flow up a plugged borehole for $\mathbf{x}_{st}$ calculated with NUTS or PANEL; this calculation requires BRAGFLO results (i.e., $f_B(\mathbf{x}_{st})$) as input, $f_{S-F}(\mathbf{x}_{st,0})$ ~ Culebra flow field calculated for $\mathbf{x}_{st,0}$ with SECOFL2D, $f_{N-P}\left[\mathbf{x}_{st}, f_B(\mathbf{x}_{st})\right]$ ~ release to Culebra for $\mathbf{x}_{st}$ calculated with NUTS or PANEL as appropriate; this calculation requires BRAGFLO results (i.e., $f_B(\mathbf{x}_{st})$) as input, $f_{S-T}\left\{\mathbf{x}_{st,0}, f_{S-F}(\mathbf{x}_{st,0}), f_{N-P}\left[\mathbf{x}_{st}, f_B(\mathbf{x}_{st})\right]\right\}$ ~ groundwater transport release through Culebra to accessible environment calculated with SECOTP2D; this calculation requires SECOFL2D results (i.e., $f_{S-F}(\mathbf{x}_{st,0})$) and NUTS or PANEL results (i.e., $f_{N-P}[\mathbf{x}_{st}, f_B(\mathbf{x}_{st})]$) as input; $\mathbf{x}_{st,0}$ is used as an argument to f_{S-T} because drilling intrusions are assumed to cause no perturbations to the flow field in the Culebra (Sect. 4, Ref. 7).

The function f_{DBR} in Eq. (1) corresponds to the model used for DBR in the 1996 WIPP PA, with the computational evaluation of this model being carried out by the BRAGFLO_DBR program (Fig. 2, Table 2, Ref. 7). As indicated in the representation for f_{DBR} in Eq. (1), calculation of the DBR involves two phase-flow results calculated by BRAGFLO[10] and spallings results calculated by CUTTINGS_S.[11] The mathematical formulations of the other functions appearing in Eq. (1) (i.e., f_B, f_C, f_{SP}, f_{MB}, f_{DL}, f_S, f_{S-T}, f_{S-F}, f_{N-P}) are described in other articles.[10-13]

The DBRs take place over a relatively short period of time (i.e., 3 to 11 days) following the drilling intrusion under consideration. The initial value conditions for use in the determination of DBRs are obtained by mapping

solutions of Eqs. (2) - (7) of Ref. 10 obtained with the computational grid in Fig. 1 of Ref. 10 onto the grid in Fig. 1 (Sect. 2).

In concept, the brine release for a drilling intrusion has the form

$$BR = \int_0^{t_e} rBR(t)dt, \tag{2}$$

where BR = brine release (m^3) for drilling intrusion, $rBR(t)$ = rate (m^3) at time t at which brine flows up intruding borehole, t = elapsed time (s) since drilling intrusion, and t_e = time (s) at which direct brine release ends. The definition of $rBR(t)$ is discussed in Sects. 3 - 6 and is based on the two-phase flow relationships in Eqs. (2) - (7) of Ref. 10 and use of the Poettmann-Carpenter correlation[14] to determine a boundary pressure at the connection between the intruding borehole and the repository. The time t_e is based on current drilling practices in the Delaware Basin (Sect. 7). The numerical solution of the equations that give rise to the brine component of the DBR is described in Sect. 8. The DBR itself is then obtained by multiplying BR by an appropriate dissolved radionuclide concentration (Sects. 9, 10).

At a conceptual level, evaluation of the CCDFs for DBRs involves evaluation of the following integral (Sect. 4, Ref. 7):

$$prob_{DBR}(Rel > R) = \int_{S_{st}} \delta_R\left[f_{DBR}\left\{\mathbf{x}_{st}, f_{SP}\left[\mathbf{x}_{st}, f_B(\mathbf{x}_{st})\right], f_B(\mathbf{x}_{st})\right\}\right] d_{st}(\mathbf{x}_{st}) dV_{st}, \tag{3}$$

where $\delta_R[f_{DBR}\{\mathbf{x}_{st}, f_{SP}[\mathbf{x}_{st}, f_B(\mathbf{x}_{st})], f_B(\mathbf{x}_{st})\}] = 1$ if $f_{DBR}\{\mathbf{x}_{st}, f_{SP}[\mathbf{x}_{st}, f_B(\mathbf{x}_{st})], f_B(\mathbf{x}_{st})\} > R$ and 0 if $f_{DBR}\{\mathbf{x}_{st}, f_{SP}[\mathbf{x}_{st}, f_B(\mathbf{x}_{st})], f_B(\mathbf{x}_{st})\} \le R$, d_{st} is the density function associated with the probability space (S_{st}, $\mathcal{S}_{st}$, p_{st}) for stochastic uncertainty, and $prob_{DBR}(Rel > R)$ is the probability that a DBR greater than size R will occur. Typically, R is expressed in the normalized units defined by the EPA (Eq. (1), Ref. 7), although other possibilities exist (e.g., m^3 when f_{DBR} is used to represent volume of brine released). In practice, the two preceding integrals are too complex to allow closed-form evaluations. As a result, the 1996 WIPP PA uses the Monte Carlo procedure indicated below to estimate this integral (Sect. 4, Ref. 7; Sects. 10, 11, Ref. 8):

$$prob_{DBR}(Rel > R) \doteq \sum_{i=1}^{nS} \delta_R\left[f_{DBR}\left\{\mathbf{x}_{st,i}, f_{SP}\left[\mathbf{x}_{st,i}, f_B(\mathbf{x}_{st,i})\right], f_B(\mathbf{x}_{st,i})\right\}\right] / nS, \tag{4}$$

where the $\mathbf{x}_{st,i}$, $i = 1, 2, \ldots, nS = 10{,}000$, correspond to a random sample of size $nS = 10{,}000$ from the sample space S_{st} associated with the probability space (S_{st}, $\mathcal{S}_{st}$, p_{st}) for stochastic uncertainty. The evaluation of the preceding approximation to produce a CCDF for DBRs is discussed in Sect. 11. The construction of CCDFs for the other release modes is discussed in other articles.[11-13,15]

When the effects of imprecisely known analysis inputs are included, a dependence on the vector $\mathbf{x}_{su}$ is added to the representation for the DBR, where $\mathbf{x}_{su}$ is an element of the sample space S_{su} associated with the probability space (S_{su}, $\mathcal{S}_{su}$, p_{su}) for subjective uncertainty (Sect. 5, Ref. 7; Ref. 9). Possible values for $\mathbf{x}_{su}$ lead to distributions of DBRs for both specific futures $\mathbf{x}_{st}$ and also for the CCDFs that result from integrating over all possible values for $\mathbf{x}_{st}$. In the 1996 WIPP PA, these distributions are approximated by using Latin hypercube sampling[16] to generate a mapping from S_{su} to analysis outcomes of interest (Sect. 5, Ref. 2; Sect. 8, Ref. 9). The generation and presentation of this mapping is usually referred to as uncertainty analysis. Once generated, this mapping can be explored with sensitivity analysis techniques based on examination of scatterplots, regression analysis, and correlation analysis (Sect. 3.5, Ref. 17). Uncertainty and sensitivity analysis results for DBRs are presented in Sects. 9 - 11. Due to the large number of zero releases, the examination of scatterplots was a more effective sensitivity analysis procedure than regression analysis and partial correlation analysis. Uncertainty and sensitivity analysis results for the other release modes are available in additional articles.[11-13, 15, 18, 19]

This article is based on material contained in Sect. 4.7 and Chapt. 10 of Ref. 20.

2. Linkage to Solution of Eqs. (2) - (7) of Ref. 10 for Two-Phase Flow

The mesh in Fig. 1 was linked to the mesh in Fig. 1 of Ref. 10 by dividing the waste disposal area in Fig. 1 into four regions (Fig. 2). Region 1 represents the farthest updip repository grid blocks in Fig. 1 of Ref. 10 that contained waste. Region 4 represents the farthest downdip repository grid blocks in Fig. 1 of Ref. 10 that contained waste and thus corresponds to the downdip waste panel. Similar subdivisions are made for regions 2 and 3. The linkage between the solutions to Eqs. (2) - (7) of Ref. 10 and the direct brine release calculations was made by assigning properties calculated by BRAGFLO for each region in Fig. 1 of Ref. 10 to the corresponding waste region in Fig. 1.

The height of the grid in Fig. 1 was assigned a value that corresponded to the crushed height h (m) of the waste as predicted by the solution of Eqs. (2) - (7) of Ref. 10. Specifically,

$$h = h_i\,(1 - \phi_i)/(1 - \phi), \tag{5}$$

where h_i and ϕ_i are the initial height (m) and porosity of the waste and ϕ is the volume-averaged porosity of the waste at the particular time under consideration as predicted by calculations with the SANTOS program (Sect. 4, Ref. 10). The areas designated panel seals, DRZ and impure halite in Fig. 1 were assigned the same pressures and saturations as the corresponding waste areas and were assigned porosities that resulted in a conservation of the initial pore volumes used for these areas in the solution of Eqs. (2) - (7) of Ref. 10 on the grid in Fig. 1 of Ref. 10 (Table 1). Specifically, the pore volumes associated with the panel seals, DRZ and impure halite do not change with time, with this constancy implemented by the definitions of $\phi(x, y, 0)$ in the lower half of Table 1.

3. Conceptual Representation for Flow Rate *rBR(t)*

The driving force that gives rise to the brine release *BR* is the difference between waste panel pressure, p_w (Pa), and the flowing bottomhole pressure in the borehole, p_{wf} (Pa), at the time of the intrusion. The flowing bottomhole pressure p_{wf}, defined as the dynamic pressure at the inlet of the intruding borehole to the waste panel, is less than the static pressure p_w due to elevation, friction and acceleration effects. The rate at which brine and gas are transported up the intruding borehole is determined by the difference $p_w - p_{wf}$ and a productivity index J_p for the intruded waste panel (p. 79, Ref. 21):

$$q_p(t) = J_p\left[p_w(t) - p_{wf}\right], \tag{6}$$

where $q_p(t)$ = flow rate (m^3/s) at time t for phase p ($p = b \sim$ brine, $p = g \sim$ gas), J_p = productivity index ($m^3/Pa{\cdot}s$) for phase p, and p_w and p_{wf} are defined above. As indicated by the inclusion/exclusion of a dependence on t, the terms J_p and p_{wf} are constant during the determination of $q_p(t)$ for a particular drilling intrusion in the present analysis, and $p_w(t)$ changes as a function of time.

The determination of J_p is now discussed. Then, the numerical determination of p_w and *BR* is discussed in Sect. 4, and the determination of p_{wf} is discussed in Sects. 5 - 6. In concept, the brine release *BR* is given by

$$BR = \int_0^{t_e} rBR(t)dt = \int_0^{t_e} J_b\left[p_w(t) - p_{wf}\right] dt \tag{7}$$

once J_p, p_w and p_{wf} are determined. The associated gas release is given by the corresponding integral with J_g rather than J_b. In the computational implementation of the analysis, *BR* is determined as part of the numerical solution of the system of partial differential equations that defines p_w (Sect. 4).

In a radial drainage area with uniform saturation, which is assumed to be valid throughout the direct brine release, the following representation for J_p can be determined from Darcy's law (p. 79, Ref. 21; Ref. 22):

$$J_p = \frac{kk_{rp}h}{\mu_p\left[\ln(r_e / r_w) + s + c\right]}, \tag{8}$$

where k = absolute permeability (assumed to be constant through time at 1.7×10^{-13} m^2), k_{rp} = relative permeability to phase p (calculated with modified Brooks-Corey model in Eqs. (11) - (12) of Ref. 10, and brine and gas saturations, S_g and S_b, obtained by mapping solutions of Eqs. (2) - (7) of Ref. 10, obtained with grid in Fig. 1 of Ref. 10, onto grid in Fig. 1), h = crushed panel height (Eq. (5)), μ_p = viscosity of fluid phase (assumed to be constant through time with $\mu_b = 1.8 \times 10^{-3}$ Pa·s, and $\mu_g = 8.92 \times 10^{-6}$ Pa·s (Ref. 23)), r_e = external drainage radius (for use with the rectangular gridblocks in Fig. 4.7.1, r_e is taken to be the equivalent areal radius; see Eq. (9)), r_w = wellbore radius (assumed to be constant through time at 0.1556 m (Table 14.7, Ref. 24)), $c = -0.50$ for pseudo steady-state

flow, and s = skin factor, which is used to incorporate flow stimulation caused by spallings release (see Eq. (10)). In the present analysis,

$$r_e = \sqrt{(10)(32.7)/\pi} = 10.2 \text{ m} \tag{9}$$

results from the gridblock dimensions of 10 m × 32.7 m for the gridblock in Fig. 1 that contains the downdip borehole.

The skin factor s is derived from the spallings release through the following petroleum engineering well testing relationship (pp. 5-7, Ref. 25):

$$s = \left(\frac{k}{k_s} - 1\right) \ln\left(\frac{r_s}{r_w}\right), \tag{10}$$

where k_S = permeability (m^2) of an open channel as a result of spallings releases (assumed to be infinite), and r_s = effective radius (m) of the wellbore with spallings volume removed. The effective radius r_s is obtained by converting the spallings volume release V_i in Eq. (39) of Ref. 11 into an equivalent areal release A_i through the relationship

$$A_i = V_i/h_i. \tag{11}$$

Then,

$$r_s = \sqrt{A_i/\pi}, \tag{12}$$

and substitution of r_s into Eq. (10) with $k_s = \infty$ yields

$$s = -\ln[\sqrt{A_i/\pi}/r_w], \tag{13}$$

which is used as the skin factor in the calculation of direct brine releases.

4. Determination of Waste Panel Pressure $p_w(t)$ and Brine Release BR

The repository pressure $p_w(t)$ in Eq. (7) after a drilling intrusion is determined with the same system of nonlinear partial differential equations discussed in Ref. 10. Indeed, what is referred to as the BRAGFLO_DBR program is actually the BRAGFLO program used with the computational grid in Fig. 1 and assumptions (i.e., parameter values, initial value conditions, and boundary value conditions) that are appropriate for representing brine flow to an intruding borehole over a relatively short time period immediately after the intrusion (i.e., 3-11 days). Due to the

short time periods under consideration, the model for direct brine release does not include gas generation due to either corrosion or microbial action and also does not include changes in repository height due to creep closure. Further, to stabilize the calculation and thus allow longer time steps in the numerical solution, the capillary pressure was assigned a value of 0 Pa in all modeled regions (Fig. 1); in the analysis of the full system in Ref. 10, capillary pressure had a value of 0 Pa in the waste regions and the DRZ but a nonzero value in the panel seals (Table 3, Ref. 10). Use of a capillary pressure of 0 Pa results in the brine pressure $p_b\,(x, y, t)$ and the gas pressure $p_g\,(x, y, t)$ being equal, with the pressure $p_w(t)$ in Eq. (7) given by

$$p_w(t) = p_b\,(x, y, t). \tag{14}$$

Although the determination of BR can be conceptually represented by the integral in Eq. (2), in the numerical implementation of the analysis BR is determined within the numerical solution of the system of partial differential equations that defines $p_b\,(x, y, t)$.

With the specific assumptions for direct brine release, Eqs. (2) - (7) of Ref. 10 become

Gas Conservation
$$\nabla \bullet \left[\frac{\alpha \rho_g \mathbf{K}_g k_{rg}}{\mu_g} \left(\nabla p_g + \rho_g g \nabla h \right) \right] = \alpha \frac{\partial \left(\phi \rho_g S_g \right)}{\partial t} \tag{15}$$

Brine Conservation
$$\nabla \bullet \left[\frac{\alpha \rho_b \mathbf{K}_b k_{rb}}{\mu_b} \left(\nabla p_b + \rho_b g \nabla h \right) \right] = \alpha \frac{\partial \left(\phi \rho_b S_b \right)}{\partial t} \tag{16}$$

Saturation Constraint
$$S_g + S_b = 1 \tag{17}$$

Capillary Pressure Constraint
$$0 = p_g - p_b \tag{18}$$

Gas Density
ρ_g determined by Redlich-Kwong-Soave equation of state (Eq. (31), Ref. 10)

Brine Density
$$\rho_b = \rho_0 \exp\left[\beta_b \left(p_b - p_{b0} \right) \right] \tag{19}$$

Formation Porosity
$$\phi = \phi_0 \exp\left[\beta_f \left(p_b - p_{b0} \right) \right] \tag{20}$$

with all symbols having the same definitions as in Eqs. (2) - (7) of Ref. 10.

The same parameter values described in Ref. 10 for the waste regions, panel seals and DRZ are used with Eqs. (15) - (20) to model direct brine releases with the following exceptions: α is a function of the computational grid and is determined by the outcome of the calculations described in Ref. 10 (i.e., $\alpha = h$ as defined in Eq. (5)), the pore distribution parameter λ used in the definition of k_{rg} and k_{rb} (see Eqs. (11) - (12), Ref. 10) is assigned a value of 0.7 for the waste regions, panel seals and DRZ (values of λ = 0.7, 0.94 and 2.89 were used for the waste regions, panel

seals and DRZ in the calculations described in Ref. 10), and the initial porosity ϕ_0 and initial pressure p_{b0} were set on the basis of the calculations described in Ref. 10 (Sect. 2). In particular, the intrinsic permeability k used in the definitions of $\mathbf{K}_g$ and $\mathbf{K}_b$ (Eq. (29), Ref. 10 is given by $k = 1.7 \times 10^{-13}$ m^2, 1.0×10^{-15} m^2 and 1.0×10^{-15} m^2 in the waste regions, panel seals and DRZ, respectively, and the relative permeabilities k_{rg} and k_{rb} are defined in Eqs. (11) - (12) of Ref. 10. The uncertain parameters residual brine saturation in waste ($WRBRNSAT \sim S_{br}$) and residual gas saturation in waste ($WRGSSAT \sim S_{gr}$) (see Table 1, Ref. 9) directly enter the direct brine release calculations through the definitions of p_C, k_{rg} and k_{rb} in Eqs. (10) - (15) of Ref. 10.

The primary differences between the BRAGFLO calculations described in Ref. 10 and the BRAGFLO_DBR calculations described in this section are in the computational meshes used (i.e., the mesh in Fig. 1 for the solution of Eqs. (15) - (20) and the mesh in Fig. 1 of Ref. 10 for the solution of Eqs. (2) - (7) of Ref. 10, the initial values used (Table 1), and the boundary values used (Table 2). In particular, the appropriate assignment of boundary value conditions is used to incorporate brine and gas flow associated with intruding boreholes into the model. Specifically, brine flow up an intruding borehole is incorporated into Eqs. (15) - (20) by using the Poettmann-Carpenter wellbore model to determine the pressure at the outflow point in a waste panel (Fig. 1), with this pressure entering the calculation as a boundary value condition (Table 2). The details of this determination are discussed in Sect. 5. Further, should a calculation involve a prior E1 intrusion, the effects of this intrusion are also incorporated into the analysis as a pressure specified as a boundary value condition (Table 2) as discussed in Sect. 6.

For perspective, the following provides a quick comparison of the assumptions that underlie the solution of Eqs. (2) - (7) of Ref. 10 on the mesh in Fig. 1 of the same article (i.e., the BRAGFLO mesh) and the solution of Eqs. (15) - (20) on the mesh in Fig. 1 (i.e., the BRAGFLO_DBR mesh): (i) The BRAGFLO_DBR mesh is defined in the areal plane with the z-dimension (height) one element thick; the BRAGFLO mesh is defined as a cross-section, with multiple layers in height and the thickness (y-dimension) one element thick. (ii) The BRAGFLO_ DBR model represents flow only in the waste area. The BRAGFLO model includes the surrounding geology as well as the entire WIPP excavation (including operations, experimental, and shaft regions). (iii) Local scale heterogeneities are included in the BRAGFLO_ DBR model, including the salt pillars, rooms, panel seals, and passageways which contain waste. These are not fully represented in the BRAGFLO mesh. (iv) The BRAGFLO_ DBR mesh uses constant thickness, while BRAGFLO rectangularly flares the element thickness to account for 3-dimensional volumes in a 2-dimensional grid (Fig. 2, Ref. 10). (v) The DRZ is included in both models, but exists above and below the excavated regions in the BRAGFLO model, whereas the DRZ surrounds the waste rooms on the sides for the BRAGFLO_ DBR model. (vi) Both models include a one degree formation dip through the excavated regions (Eq. 9), Ref. 10.

5. Boundary Value Pressure p_{wf}

The boundary value pressure p_{wf} at the inlet of the intruding borehole is defined by a system of equations of the following form:

$$dp/dh = F\ \{q_b[p(0)],\ q_g[p(0)],\ p(h),\ h\},\ 0 \le h \le 655\ \text{m} \tag{21}$$

$$p(655) = 1.013 \times 10^5\ \text{Pa} \tag{22}$$

$$q_b[p(0)] = J_b[p_w - p(0)] \tag{23}$$

$$q_g[p(0)] = J_g[p_w - p(0)], \tag{24}$$

where $p(h)$ is pressure (Pa) at elevation h (m) in the borehole with h = 0 m corresponding to the entry point of the borehole into the waste panel and h = 655 m corresponding to the land surface (Fig. 3), F is a function (Pa/m) characterizing the change of pressure with elevation in the borehole, $p(655)$ is an initial value condition requiring that pressure at the land surface (i.e., the outlet point of the borehole) be equal to atmospheric pressure, $q_b[p(0)]$ and $q_g[p(0)]$ define brine and gas flow rates (m^3/s) into the borehole (see Eq. (6)), J_b and J_g are productivity indexes (m^3/Pa s) (see Eq. (8)), and p_w is the pressure (Pa) in the repository at the time of the drilling intrusion.

The boundary value pressure p_{wf} is defined by

$$p_{wf} = p(0). \tag{25}$$

Thus, p_{wf} is determined by the numerical solution of Eq. (21) for $p(0)$ subject to the constraints in Eqs. (22) - (24).

The pressure p_w corresponds to the pressure $p_w(0)$ in Eq. (14) and is obtained from the solution of Eqs. (2) - (7) of Ref. 10 with the computational grid in Fig. 1 of the same article (see Sect. 2). The production indexes J_b and J_g are defined in Eq. (8). Thus, the only quantity remaining to be specified in Eqs. (21) - (24) is the function F.

Brine and gas flow up a borehole is governed by complex physics dependent on frictional effects and two-phase fluid properties. This phenomena has been widely studied in the petroleum industry and many modeling procedures (i.e., empirical correlations) have been developed to predict flow rates and pressures in vertical two-phase pipe flow (i.e., to define F in Eq. (21)).[26] For this analysis, the Poettmann-Carpenter model[14, 27] was used to define F because it accounts for multi-phase frictional effects based on empirical (i.e., field) data from flowing wells, is one of the few modeling approaches that included annular flow data in its development, and is relatively easy to implement. Specifically, the Poettmann-Carpenter model defines F by

$$F\{q_b[p(0)],\ q_g[p(0)],\ p(h), h\} = gm(h) + f'\{m(h), D(h), q_b[p(0)]\} gm(h) F^2(h) / D^5(h), \tag{26}$$

where g = acceleration due to gravity (9.8 m/s^2), $m(h)$ = density (kg/m^3) of fluids (i.e., gas and brine) in wellbore at elevation h (Note: $m(h)$ is a function of $q_b[p(0)]$ and $q_g[p(0)]$; see Eq. (27) below), $f'\{m(h), D(h)q_b[p(0)]\}$ = empirically defined scale factor (m/s^2) (Note: f' is the scale factor in the Poettmann-Carpenter model for fluid flow in a wellbore[14]; see discussion below), $F(h)$ = flow rate (m^3/s) of fluids (i.e., gas and brine) in wellbore at elevation h (Note: $F(h)$ is a function of q_b $[p(0)]$ and q_g $[p(0)]$; see Eq. (28) below), and $D(h)$ = effective diameter (m) of wellbore (see Eq. (31) below). The first term, $gm(h)$, in Eq. (26) results from the contribution of elevation to pressure; the second term results from frictional effects.[14] The original development of Eq. (26)[14] and also the numerical implementation in the 1996 WIPP PA[6] used oilfield units. However, for consistency with the other model descriptions in this presentation, the terms in this equation are given in SI units.

The fluid density $m(h)$ at elevation h is given by

$$m(h) = \{q_b[p(0)]\rho_b[p(0)] + q_g[p(0)]\rho_g[p(0)]\} / F(h), \tag{27}$$

where

$$F(h) = q_b[p(0)] + [z(h)p(h) / p(0)]q_g[p(0)], \tag{28}$$

$\rho_b[p(0)$ = density (kg/m^3) of brine at pressure $p(0)$ and temperature 300.1°K, which is fixed at 1230 kg/m^3, $\rho_g[p(0)]$ = density (kg/m^3) of H_2 at pressure $p(0)$ and temperature 300.1°K (see Eq. (29) below), and $z(h)$ = z-factor for compressibility of H_2 at elevation h (Note: $z(h)$ is a function of $p(h)$; see Eq. (30) below), and $q_b[p(0)]$ and $q_g[p(0)]$ are defined in Eqs. (23) and (24). The gas density in Eq. (27) is obtained from the universal gas law, $PV = nRT$, by

$$\rho_g[p(0)] = C_{m,kg}(n / V) = C_{m,kg}(P / RT), \tag{29}$$

where n is the amount of gas (mol) in a volume V, $C_{m,kg}$ is the conversion factor from moles to kilograms for H_2 (i.e., 2.02×10^{-3} kg/mol), $P = p(0)$, $R = 8.3145$ kg m^2/mol°K s^2, and $T = 300.1$°K. The Z-factor is given by

$$z(h) \doteq 1 + (8.54 \times 10^{-8} Pa^{-1})p(h) \tag{30}$$

and was obtained from calculations performed with the SUPERTRAPP program[28] for pure H_2 and a temperature of 300.1°K (Fig. 4.7.4, Ref. 6). The preceding approximation to $Z(h)$ was obtained by fitting a straight line between the results for pressures of 0 psia and 3000 psia and a hydrogen mole fraction of 1 in Fig. 4.7.4 of Ref. 6; the actual calculations used the more complex, but numerically similar, regression model given in Fig. 4.7.4 of Ref. 6. The numerator and denominator in Eq. (27) involve rates, with the time units canceling to give $m(h)$ in units of kg/m^3.

The effective diameter $D(h)$ in Eq. (26) is defined with the hydraulic radius concept. Specifically,

$$D^5(h) = [D_i(h) + D_o(h)]^2 [D_i(h) - D_o(h)]^3 , \tag{31}$$

where $D_i(h)$ and $D_o(h)$ are the inner and outer diameters (m) of the wellbore at elevation h(m) (see Fig. 3).

The factor f' in Eq. (26) is a function of $m(h)$, $D(h)$ and $q_b[p(0)]$. In the original development by Poettmann and Carpenter (Fig. 4, Ref. 14), f' is defined in terms of quantities commonly used to measure production from oil and gas wells (Note: Poettmann and Carpenter use the symbol f rather than the symbol f' used in many subsequent treatments). The result is that f' is expressed in quantities that are unfamiliar outside of the oil and gas industry. For clarity, Eq. (26) and the quantities contained in it are expressed in SI units. However, to allow use of the original correlations developed by Poettmann and Carpenter to define f', the calculations within the 1996 WIPP PA[6] were performed in the same oilfield units originally used by Poettmann and Carpenter.

The following iterative procedure based on Euler's method was used to approximate solutions to Eqs. (21) - (24) for $p(0)$:

Step 1. Make initial or updated estimate of $p(0)$ as appropriate. (Initial guess for $p(0)$ is midpoint $p_w/2$ of interval $[0, p_w]$, where p_w is the pressure in the repository at the time of the drilling intrusion used in Eqs. (23), (24). Next guess for $p(0)$ is at midpoint of $[0, p_w/2]$ or $[p_w/2, p_w]$ depending on whether resultant approximation to $p(655)$ is above or below atmospheric pressure. Subsequent guesses for $p(0)$ are made in a similar manner.

Step 2. Use $p(0)$, known values for J_b, J_g and p_w, and Eqs. (23) - (24) to determine $q_b[p(0)]$ and $q_g[p(0)]$.

Step 3. Use Euler's method with Δh = 25 ft = 7.62 m and appropriate changes in annular diameter (Fig. 3) to determine $p(655)$ [i.e., $p(h + \Delta h) = p(h) + F\{q_b[p(0)], q_g[p(0)], p(h), h\}\Delta h$].

Step 4. Stop if $p(655)$ is within 0.07% of atmospheric pressure (i.e., if $|1.013 \times 10^5 \text{ Pa} - p(655)| \leq 71$ Pa). Otherwise, return to Step 1 and repeat process.

The preceding procedure is continued until the specified error tolerance (i.e., 0.07%) has been met or 26 iterations have been performed. If the specified error tolerance has not been met after 26 iterations, the procedure is repeated with the error tolerance increased to 5%.

The computational design of the 1996 WIPP PA had the potential to require 15,600 separate direct brine release calculations (Sect. 13, Ref. 8). In concept, each of these cases requires the solution of Eqs. (21) - (24) with the iterative procedure just presented to obtain the boundary value condition $p_{wf} = p(0)$ for use in conjunction with Eqs. (15) - (20) (Table 2). To help hold computational costs down, Eqs. (21) - (24) were solved for $p(0)$ for approximately 2000 randomly-generated vectors of the form

$$\mathbf{v} = [p_w, h, S_{br}, S_{gr}, S_b, A_i], \tag{32}$$

where p_w is the repository pressure (used in definition of $q_b[p(0)]$, $q_g[p(0)]$ in Eqs. (23), (24)), h is the crushed height of the repository (used in definition of J_p in Eq. (8)), S_{br} and S_{gr} are the residual saturations for gas and brine in the repository (used in definition of k_{rp} in Eq. (8)), S_b is the saturation of brine in the repository (used in definition of k_{rp} in Eq. (8)), and A_i is the equivalent area of material removed by spallings (used in definition of skin factor s in Eq. (13)). The outcomes of these calculations were divided into three cases: (1) mobile brine only (i.e., $k_{rg} = 0$ in Eq. (12), Ref. 10), (2) brine-dominated flow (i.e., $\log (k_{rg}/k_{rb}) \leq 0$), and (3) gas-dominated flow (i.e., $\log (k_{rg}/k_{rb}) > 0$). Then, regression procedures were used to fit algebraic models that can be used to estimate $p(0)$ (Figs. 4 - 6). These regression models were then used to determine $p(0)$, and hence p_{wf}, in the 1996 WIPP PA.

6. Boundary Value Pressure p_{wE1}

Some of the calculations for direct brine release are for a drilling intrusion that has been preceded by an E1 intrusion in either the same waste panel or a different waste panel (Sect. 12, Ref. 8). The effects of these prior E1 intrusions are incorporated into the solution of Eqs. (15) - (20), and hence into the direct brine release *DBR*, by the specification of a boundary pressure p_{wE1} at the location of the E1 intrusion into the repository (Table 2).

Two cases are considered for the definition of p_{wE1}: (1) an open borehole between the brine pocket and the repository, and (2) a borehole between the brine pocket and the repository filled with material with properties similar to silty sand. The first case corresponds to the situation in which the drilling intrusion under consideration has occurred within 200 yr of a prior drilling intrusion that penetrated the pressurized brine pocket, and the second case corresponds to the situation in which the drilling intrusion under consideration has occurred more than 200 yr after a prior drilling intrusion that penetrated the pressurized brine pocket (Table 8, Ref. 10).

Case 1: Open Borehole. A derivation follows for the flowing well pressure at the inlet to the repository associated with a drilling intrusion that penetrates the repository and a brine pocket under the assumption that an open borehole exists between the brine pocket and the repository. The value for this pressure is then assigned to p_{wE1} for the case under consideration (Table 2). This determination is made by developing a system of equations of the following form:

$$Q = f_1 (p_{BP}, p_{wfBP}) \tag{33}$$

$$Q = f_2 (p_{wfBP}, p_{wfBI}) \tag{34}$$

$$Q = f_3 (p_{wfBI}, p_{wfBO}), \tag{35}$$

where p_{BP} = pressure (Pa) in brine pocket, p_{wfBP} = flowing well pressure (Pa) at outlet from brine pocket, p_{wfBI} = flowing well pressure (Pa) at inlet to repository from brine pocket, p_{wfBO} = flowing well pressure (Pa) at outlet from repository due to intruding borehole (Note: The boreholes associated with p_{wfBI} and p_{wfBO} arise from different

drilling intrusions and hence are at different locations; see Fig. 1), Q = brine flow rate (m^3/s) from brine pocket to repository, through repository, and then to surface, and f_1, f_2 and f_3 are linear functions of their arguments. In the development, p_{BP} and p_{wfBO} are assumed to be known, with the result that Eqs. (33) - (35) constitute a system of three linear equations in three unknowns (i.e., p_{wfBP}, p_{wfBI}, Q) that can be solved to obtain p_{wfBI}. In the determination of $p_{wfBI} = p_{wE1}$ for use in a particular solution of Eqs. (15) - (20), p_{BP} is the pressure in the brine pocket at the time of the intrusion obtained from the solution of Eqs. (2) - (7) of Ref. 10 with BRAGFLO, and p_{wfBO} is the flowing well pressure obtained from conditions at the time of the intrusion (from the solution of Eqs. (2) - (7), Ref. 10) and the solutions of the Poettmann-Carpenter model embodied in Figs. 4 - 6. (i.e., given pressure, k_{rg} and k_{rb} at the time of the intrusion from the solution of Eqs. (2) - (7) of Ref. 10 with BRAGFLO and J_b from both the solution of Eqs. (2) - (7) of Ref. 10 with BRAGFLO and the evaluation of the spallings release with CUTTINGS_S, p_{wfBO} is determined from the regression models indicated in Figs. 4 - 6).

The definition of Eqs. (33) - (35) is now discussed. Eq. (33) characterizes flow out of the brine pocket into an open borehole and has the form[22]

$$Q = \left(\frac{k_{BP} h_{BP}}{\mu [\ln(r_{eBP} / r_w) - 0.5]} \right) \left(p_{BP} - p_{wfBP} \right), \tag{36}$$

where k_{BP} = brine pocket permeability (m^2), h_{BP} = effective brine pocket height (m), r_{eBP} = effective brine pocket radius (m), r_w = wellbore radius (m), and μ = brine viscosity (Pa s). In the present analysis, k_{BP} is an uncertain analysis input (see *BPPRM* in Table 1, Ref. 9), h_{BP} = 12.34 m,[6] r_{eBP} = 114 m,[6] which corresponds to the size of the largest brine pocket that could fit under one waste panel, r_w = (8.921 in) /2 = 0.1133 m, which is the inside radius of a 9-5/8 inch outside diameter casing (Table 14.7, Ref. 24), $\mu = 1.8 \times 10^{-3}$ Pa s, and p_{BP} is determined from the solution of Eqs. (2) - (7) of Ref. 10 as previously indicated.

Eq. (34) characterizes flow up an open borehole from the brine pocket to the repository and is based on Poiseuille's Law (Eqs. 7-21, 7-22, Ref. 29). Specifically, Eq. (34) has the form

$$Q = \left[\frac{\pi D^4}{128 \mu (y_{BP} - y_{rep})} \right] \left[\left(p_{wfBP} - p_{wfBI} \right) + g\rho \left(y_{rep} - y_{BP} \right) \right], \tag{37}$$

where D = wellbore diameter (m), y_{rep} = elevation of repository (m) measured from surface, y_{BP} = elevation of brine pocket (m) measured from surface, g = acceleration due to gravity (9.8 m/s^2), ρ = density of brine (kg/m^3), and the remaining symbols have already been defined.

In the present analysis, D = $2r_w$ = 0.2266 m, ρ = 1230 kg/m^3, and $y_{rep} - y_{BP}$ = 247 m. With the preceding values,

$$128\mu(y_{BP} - y_{rep})/\pi D^4 = 6.87 \times 10^3 \text{ Pa s/m}^3 \tag{38}$$

$$g\rho(y_{rep} - y_{BP}) = -2.98 \times 10^6 \text{ Pa.} \tag{39}$$

Thus,

$$p_{wfBI} \doteq p_{wfBP} - 2.98 \times 10^6 \text{ Pa} \tag{40}$$

when Q is small (≤ 0.1 m^3/s). When appropriate, this approximation can be used to simplify the construction of solutions to Eqs. (33) - (35).

Eq. (35) characterizes flow from the brine pocket inlet point to the repository to the outlet point associated with the drilling intrusion under consideration and has the same form as Eq. (36). Specifically,

$$Q = \left(\frac{k_{rep} h_{rep}}{\mu[\ln(r_{e,rep} / r_w) - 0.5]} \right) \left(p_{wfBI} - p_{wfBO} \right), \tag{41}$$

where k_{rep} = repository permeability (m^2), h_{rep} = repository height (m), $r_{e,rep}$ = effective repository radius (m), and the remaining symbols have already been defined. In the present analysis, $k_{rep} = 1.7 \times 10^{-13}$ m^2; h_{rep} at the time of the drilling intrusion under consideration is obtained from the solution of Eqs. (2) - (7) of Ref. 10 (see Eq. (5)); and $r_{e,rep}$ is the same as the radius r_e defined in Eq. (9) (i.e., $r_{e,rep} = 10.2$ m). As previously indicated, p_{wfBO} is obtained from the solutions to the Poettmann-Carpenter model summarized in Figs. 4 - 6.

Three equations (i.e., Eqs. (36), (37) and (41)) in three unknowns (i.e., p_{wfBP}, p_{wfBI} and Q) have now been developed. Solution is straight forward (e.g., use Cramer's Rule or a simple numerical procedure). It is the solution for p_{wfBI} that is of primary interest because p_{wfBI} defines the initial value p_{wE1} in Table 2. When the simplification in Eq. (40) is used, the resultant solution for p_{wfBI} is

$$p_{wfBI} = (p_{wfBO} + K_1 p_{BP} - 2.98 \times 10^6 K_1) / (1 + K_1), \tag{42}$$

where

$$K_1 = \{k_{BP} h_{BP} \ln[(r_{e,rep} / r_w) - 0.5]\} / \{k_{rep} h_{rep} \ln[(r_{eBP} / r_w) - 0.5]\} \tag{43}$$

and -2.98×10^6 comes from Eq. (39). The expression in Eq. (43) was used to define p_{wE1} in the 1996 WIPP PA in the determination of direct brine releases for a drilling intrusion that occurred within 200 yr of a preceding E1 intrusion (see Table 8, Ref. 10).

Case 2: Sand-Filled Borehole. The determination of the pressure p_{wfBI} in Fig. 9 with the assumption that a borehole filled with material with properties similar to silty sand connects the brine pocket and the repository is now considered. The approach is similar to that used for the open borehole except that Eqs. (33) - (34) are replaced by a single equation based on Darcy's Law. Specifically, flow from the brine pocket to the repository is represented by

$$Q = k_{BH} A_{BH} [(p_{wfBP} - p_{wfBI}) + g\rho(y_{rep} - y_{BP})] / [\mu(y_{BP} - y_{rep})], \tag{44}$$

where k_{BH} = borehole permeability (m^2), A_{BH} = borehole cross-sectional area (m^2), and the remaining symbols have been defined previously. In the present analysis, k_{BH} is an uncertain input (see *BHPRM* in Table 1, Ref. 9) and A_{BH} is defined by the assumption that the borehole diameter is the same as the drillbit diameter (i.e., 12.25 in. = 0.311 m).

The representation for flow from the brine pocket inlet point to the repository to the outlet point associated with the drilling intrusion under consideration remains as defined in Eq. (41). Thus, two equations (i.e., Eqs. (44) and (41)) and two unknowns (i.e., p_{wfBI} and Q) are under consideration. Solution for p_{wfBI} is straight forward and yields

$$p_{wfBI} = (p_{wfBO} + K_2 p_{BP} - 2.98 \times 10^6 K_2) / (1 + K_2), \tag{45}$$

where

$$K_2 = \pi k_{BH} r_w^2 [\ln(r_{eBP} / r_w) - 0.5] / [h_{rep} k_{rep} (y_{BP} - y_{rep})] \tag{46}$$

and -2.98×10^6 comes from Eq. (39). The expression in Eq. (45) was used to define p_{wE1} in the determination of direct brine releases for a drilling intrusion that occurred more than 200 yr after a preceding E1 intrusion (see Table 8, Ref. 10).

7. End of Direct Brine Release t_e

The 1996 WIPP PA involved 15,600 cases that potentially required solution of Eqs. (15) - (20) to obtain the direct brine release *DBR* (Sect. 12, Ref. 8). However, the direct brine release was set to zero without solution of Eqs. (15) - (20) when there was no possibility of a release (i.e., the intruded waste panel at the time of the intrusion had either a pressure less than 8 MPa or a brine saturation below the residual brine saturation S_{br}, which was defined by the uncertain analysis input *WRBRNSAT* (see Table 1, Ref. 9).

For the remaining cases, Eqs. (15) - (20) were solved for a time period of 50 days, although the value used for t_e was always less than 50 days. The minimum value used for t_e was 3 days, which is an estimate of the time required to drill from the repository through the Castile Fm and then cement the intermediate casing. If there is little or no gas

flow associated with brine inflow into the borehole during drilling in the Salado Fm, current industry practice is to allow the brine to "seep" into the drilling mud and be discharged to the mud pits until the salt section is cased.

If there is a significant amount of gas flow, then it is possible that the driller will lose control of the well. In such cases, direct brine releases will take place until the gas flow is brought under control. Two possibilities exist: (1) the driller will regain control of the well when the gas flow drops to a manageable level, and (2) aggressive measures will be taken to shut off the gas flow before it drops to a manageable level. In the 1996 WIPP PA, the driller was assumed to be able to regain control of the well when the gas flow dropped to a "cut-off" rate of 1×10^5 standard cubic feet per day (SCF/d in commonly used oil field units). Experience at the South Culebra Bluff Unit #1, which blew out in January 1978, suggests that approximately 11 days are needed to bring a well under control before the gas flow drops to a manageable level (i.e., 1×10^5 SCF/d). In particular, 11 days was the time required to assemble the necessary equipment and personnel and then bring that well under control.

Given the preceding, t_e is defined by

$$t_e = \begin{cases} \max\{3\text{ d}, t_f\} & \text{if } t_f \le 11\ d \\ 11\ d & \text{if } t_f > 11\ d \end{cases} \tag{47}$$

in the 1996 WIPP PA, where t_f is the time at which the gas flow out of the well drops below 1×10^5 SCF/d. As a reminder, gas flow out of the repository in the intruding borehole, and hence t_f, is determined as part of the solution to Eqs. (15) - (20).

8. Numerical Solution

As previously indicated, the BRAGFLO_DBR program used to solve Eqs. (15) - (20) is just the BRAGFLO program used with the computational grid in Fig. 1, the initial value and boundary value conditions in Tables 1 and 2, and parameter values appropriate for modeling direct brine releases. Thus, the numerical procedures in use are the same as those described in Sect. 9 of Ref. 10 for the solution of Eqs. (2) - (7) of the same article.

In this solution, the boundary value conditions associated with drilling intrusions (i.e., p_{wf} and p_{wE1} in Table 2) are implemented through the specification of fluid withdrawal terms (i.e., q_{wg} and q_{wb} in Eqs. (2) and (3) of Ref. 10 rather than as defined boundary value conditions. With this implementation, the representations in Eqs. (15) and (16) for gas and brine conservation become

$$\nabla \bullet \left[\frac{\alpha \rho_g \mathbf{K}_g k_{rg}}{\mu_g} \left(\nabla p_g + \rho_g g \nabla h \right) \right] + \alpha q_{wg} = \alpha \frac{\partial \left(\phi \rho_g S_g \right)}{\partial t} \tag{48}$$

$$\nabla \bullet \left[\frac{\alpha \rho_b \mathbf{K}_b k_{rb}}{\mu_b} \left(\nabla p_b + \rho_b g \nabla h \right) \right] + \alpha q_{wb} = \alpha \frac{\partial \left(\phi \rho_b S_b \right)}{\partial t} \tag{49}$$

and the constraints in Eqs. (17) - (20) remain unchanged. All quantities appearing in Eqs. (17) - (20), (48), (49) except q_{wg} and q_{wb} have been defined (see paragraph following Eqs. (15) - (20)).

The definitions of q_{wg} and q_{wb} are now considered. As used in Eqs. (48) and (49), q_{wg} and q_{wb} are independent of the computational grid in use (Fig. 1). In practice, q_{wg} and q_{wb} are defined with a productivity index (see Eq. (8)) that is a function of the specific computational grid in use, with the result that these definitions are only meaningful in the context of the computational grid that they are intended to be used with. This specificity results because q_{wg} and q_{wb} as used in Eqs. (48) and (49) are defined on a much smaller scale than can typically be implemented with a reasonable-sized computational grid. As a result, the values used for q_{wg} and q_{wb} in the numerical solution of Eqs. (48) and (49) must incorporate the actual size of the grid in use.

In the solution of Eqs. (48) and (49) with the computational grid in Fig. 1, q_{wg} is used to incorporate gas flow out of the repository and q_{wb} is used to incorporate both brine inflow to the repository from a pressurized brine pocket and brine flow out of the repository. For gas flow out of the repository,

$$q_{wg}(x,y,t) = \frac{k k_{rg}(x,y,t)[p_g(x,y,t) - p_{wf}]}{\mu_g[\ln(r_e / r_w) + s + c]} \tag{50}$$

if (x, y) is at the center of the grid cell containing the drilling intrusion (Fig. 1) and q_{wg} $(x, y, t) = 0$ $(\mathrm{kg/m^3})/\mathrm{s}$ otherwise, where k, k_{rg}, μ_g, r_e, r_w, s and c are defined in conjunction with Eq. (8), p_g is gas pressure, and p_{wf} is the flowing well pressure at the outlet borehole (i.e., the boundary value condition in Table 2). The factor h in Eq. (8) is the crushed height of the repository as indicated in Eq. (5) and defines the factor α in Eqs. (48) and (49). In the numerical solution of Eqs. (48) and (49), $q_{wg}(x, y, t)$ defines $q^{n+1}_{wgi,j}$ in Eq. (73) of Ref. 10, with $q^{n+1}_{wgi,j}$ having a nonzero value only when i, j correspond to the grid cell containing the borehole through which gas outflow is taking place (i.e., the grid cells containing the down-dip and up-dip wells in Fig. 1).

For brine flow,

$$q_{wb}(x,y,t) = \frac{k k_{rb}(x,y,t)[p_b(x,y,t) - p_{wf}]}{\mu_b[\ln(r_e / r_w) + s + c]} \tag{51}$$

if (x, y) is at the center of the grid cell containing the drilling intrusion through which brine outflow from the repository is taking place (Fig. 1);

$$q_{wb}(x,y,t) = \frac{k k_{rb}(x,y,t)[p_{wE1} - p_b(x,y,t)]}{\mu_b[\ln(r_e / r_w) + c]} \tag{52}$$

if (x, y) is at the center of the grid cell containing a prior drilling intrusion into a pressurized brine pocket (Fig. 1), where p_{wE1} is the boundary value condition defined in Table 2; and $q_{wb}(x, y, t) = 0$ otherwise. In the numerical solution of Eqs. (48) and (49), $q_{wb}(x, y, t)$ defines $q^{n+1}_{wbi,j}$ in a discretization for Eq. (49) that is equivalent to the discretization for Eq. (48) shown in Eq. (73) of Ref. 10; with $q^{n+1}_{wbi,j}$ having a nonzero value only when i, j correspond to the grid cell containing the borehole through which brine outflow is taking place (i.e., the grid cells containing the down-dip and up-dip wells in Fig. 1; in which case, Eq. (51) defines $q^{n+1}_{wbi,j}$) or to the grid cell containing the borehole through which brine inflow to the repository from a pressurized brine pocket is taking place (i.e., the grid cell containing the E1 intrusion in Fig. 1; in which case, Eq. (53) defines $q^{n+1}_{wbi,j}$).

Additional information on BRAGFLO_DBR (actually BRAGFLO) and its use in the 1996 WIPP PA to determine direct brine releases can be found in the analysis package for direct brine release[6] and in the BRAGFLO users manual.[30]

9. Direct Brine Release: Uncertainty and Sensitivity Analysis

The direct brine release model predicts time-dependent releases of brine and gas (Figs. 7 and 11, Ref. 6). For a given drilling intrusion, the volume of released brine (m^3) is multiplied by the concentration (EPA units/m^3) of dissolved radionuclides in CH-TRU waste (Sect. 10) at the time of the intrusion to produce the direct brine release. Prior to an E1 intrusion, solubilities associated with brines derived from the Salado Fm are used; after an E1 intrusion, solubilities associated with brines derived from the Castile Fm are used. Due to the low permeability of the region surrounding each RH-TRU waste canister, intrusions into RH-TRU waste are assumed not to produce direct brine releases.

The amount of brine associated with a direct brine release is sensitive to both the pressure and brine saturation in the vicinity of the drilling intrusion. In turn, pressure and saturation are dependent on both the time of a drilling intrusion and whether or not the drilling intrusion has been preceded by earlier intrusions. Due to the 1° dip of the repository, it is also possible that conditions influencing direct brine release may differ between upper panels (i.e., panels 1, 2, 3, 6, 7, 8, 9 in Fig. 1, Ref. 8) and lower panels (i.e., panels 4, 5, 10 in Fig. 1, Ref. 8).

The preceding considerations involving the time and location of drilling intrusions also affect spallings releases. Therefore, direct brine release calculations were performed for the same times as spallings calculations (Sect. 12, Ref. 8). Specifically, direct brine release calculations were performed for initial intrusions at 100, 350, 1000, 3000, 5000 and 10,000 yr and also for intrusions into upper (U) and lower (L) waste panels (Fig. 7). Most of the LHS elements indicated in Eq. (14) of Ref. 9 for replicates R1, R2 and R3 produce no releases. Further, most of the nonzero releases occurred for intrusions into the lower waste panel.

Examination of the results for intrusion into the lower waste panel shows that nonzero brine releases tend to be associated with larger values for brine saturation and intermediate values for pressure (Fig. 8). The largest gas pressures tend to be associated with low brine saturations (Fig. 9) due to the consumption of brine in the corrosion of steel and hence result in no direct brine releases. As pressure is almost constant throughout the repository (Fig. 29, Ref. 19), the greater number of zero releases for intrusions into the upper waste panels is due to lower brine saturation (Fig. 23, Ref. 18). When a nonzero brine release does occur, the size of the corresponding normalized release tends to increase as the dissolved radionuclide concentration in the brine increases (Fig. 10).

An alternate way to view the results in Figs. 8 and 9 is to use three dimensional plots. Then, the interplay between brine release, saturation and pressure can be seen in a single plot (Fig. 11).

Direct brine release calculations were also performed for intrusions subsequent to an initial intrusion for the same intrusion combinations as used for spallings (Fig. 12). As for initial intrusions, most LHS elements result in no brine release for second intrusions. Due to the effects of the brine pocket, intrusions subsequent to an E1 intrusion tend to have more nonzero releases than intrusions subsequent to an E2 intrusion. Further, intrusions into the same waste panel tend to result in larger releases than intrusions into different waste panels. As pressure is almost constant throughout the repository (Fig. 29, Ref. 19), the greater number of zero releases from intrusions into different waste panels is due to lower brine saturation. However, it should be recognized that, in the computational implementation of the analysis, what is described as two intrusions into the same panel is actually two intrusions into the same lower panel, and what is described as two intrusions into different panels actually consists of an initial intrusion into a lower waste panel and a subsequent intrusion into an upper waste panel (Fig. 1).

Borehole permeability (i.e., $k = 10^x$, $x = BHPRM$), brine saturation and repository pressure interact to determine the volume of brine released by a second drilling intrusion (Fig. 13). Specifically, direct brine releases for second intrusions tend to be associated with higher brine saturations, higher pressures, and lower borehole permeabilities. Further, the higher pressures tend to be associated with the lower borehole permeabilities (Fig. 32, Ref. 19). High brine saturations are often associated with high values for borehole permeability (Figs. 36, 37, Ref. 19). However, this combination of high saturation and high borehole permeability does not result in a spallings release for a second or subsequent intrusion because the repository pressure is too low (Fig. 32, Ref. 19).

10. Solubility: Uncertainty and Sensitivity Analysis

Given that a nonzero brine release takes place, radionuclide solubility is a major determinant of the size of a direct brine release (Fig. 10). The solubilities used in determining a direct brine release (see S_T in Table 1, Ref. 12) depend on whether the conditions in the repository are dominated by brine from the Salado Fm (Fig. 14a) or brine from the Castile Fm (Fig. 14b). For the 1996 WIPP PA, releases from a previously unintruded repository and also releases not preceded by an E1 intrusion use the Salado-dominated solubilities; releases after an E1 intrusion use the

Castile-dominated solubilities. Thus, the normalized releases in Figs. 7b and 12d were calculated with the appropriate time-dependent solubilities from Fig. 14a; similarly, the normalized releases in Fig. 12b were calculated with the appropriate time-dependent solubilities from Fig. 14b.

Each curve in Fig. 14 results from one LHS element and derives from the values of several uncertain variables as indicated in Table 1 of Ref. 12. The noticeable downward shift of the solubility curves in Fig. 14 results when the number of EPA units in solution changes from being dominated by Am-241 to being dominated by Pu-239. A similar but less conspicuous shift also takes place at earlier times in Fig. 14a when the number of EPA units in solution changes from being dominated by Pu-238 to being dominated by Am-241.

For the 1996 WIPP PA, MgO is assumed to be added to the waste panels as a backfill to remove CO_2 generated by microbial action and thereby to reduce solubilities by increasing the pH in the waste panels. In the absence of MgO, radionuclide solubilities tend to be higher (Fig. 15). The real difference between the solubilities in Figs. 14 and 15 is not the presence or absence of MgO in the repository but rather the presence or absence of CO_2 produced by microbial degradation of cellulosics.[31]

The maximum solubilities in the absence of MgO are increased relative to the maximum solubilities in the presence of MgO. However, the minimum solubilities with and without MgO are similar. This pattern occurs because a degree of belief probability of 0.5 was assigned to the occurrence of the microbial degradation of cellulose in the 1996 WIPP PA (see *WMICDFLG* in Table 1, Ref. 9). As a result, the presence or absence of MgO has no effect on the solubilities associated with half of the LHS elements because no microbial degradation of celluloses is assumed to be equivalent to the absence of CO_2, which results in half the solubility curves in Fig. 15 being identical to curves for the corresponding LHS elements in Fig. 14. Specifically, if microbial degradation of cellulose does not take for a given LHS element, then the presence or absence of MgO does not affect the solubilities for that element. The presence or absence of microbial degradation is the cause of the two groups of solubility curves in Fig. 15b.

11. Direct Brine Release: CCDFs

As for cuttings and spallings (Sects. 5, 10, Ref. 11), each Latin hypercube sample (LHS) element leads to a CCDF for direct brine releases that is obtained by randomly sampling futures from the probability space (S_{st}, δ_{st}, p_{st}) associated with stochastic uncertainty (Sect. 10, Ref. 8) and then constructing the corresponding direct brine release for each future. This construction is based on the volumes of brine (m^3) brought to the surface by direct brine release under different conditions and the radionuclide concentration (EPA units/m^3) in that brine (Table 3). The structure of the results in Table 3 for brine releases is the same as the structure of the results in Table 2 of Ref. 11 for solid material releases.

For each sampled intrusion time, radionuclide concentration can be obtained by interpolating on $C_{E0}(\tau_k)$ and $C_{E1}(\tau_k)$ as appropriate (Table 3). Specifically, $C_{E0}(\tau_k)$ is used before any Castile brine has entered the repository due to an E1 intrusion, and $C_{E1}(\tau_k)$ is used after an E1 intrusion has allowed Castile brine to enter the repository. Further, for an initial intrusion, the volume of released brine can be obtained by interpolating on $VB_{E0,U}(\tau_k)$ and $VB_{E0,L}(\tau_k)$.

As for spallings, obtaining results for second and subsequent intrusions is more difficult for two reasons. First, results are available for initial intrusions at only 350 and 1000 yr. Second, results are available for second intrusions but not for subsequent intrusions. The availability of results for initial intrusions at only 350 and 1000 yr is handled by extending these results to initial intrusions at other times on the basis of the assumption that elapsed time from the first to the second intrusion (i.e., $\Delta\tau_{jk}$) is the primary determinant of the direct brine release for the second intrusion. Specifically, the following assignments are made:

$$VB_{E1,S}(\tau, \Delta\tau_{1k}) = VB_{E1,S}(\tau_1, \Delta\tau_{1k}) \tag{53}$$

for $100 \le \tau \le \tau_1 = 350$ yr, and

$$VB_{E1,S}(\tau, \Delta\tau_{2k}) = VB_{E1,S}(\tau_2, \Delta\tau_{2k}) \tag{54}$$

for $\tau_2 = 1000 \le \tau \le 10{,}000$ yr. Similar assignments are also made for $VB_{E1,D}$, $VB_{E2,S}$ and $VB_{E2,D}$. The lack of results for more than two intrusions is handled by assuming that direct brine releases for third and subsequent intrusions can be estimated by ignoring intermediate intrusions and treating the initial intrusion and the particular subsequent intrusion under consideration as if they were the only two intrusions in existence (Table 4).

For each LHS element, nS = 10,000 futures are randomly selected (Sect. 10, Ref. 8) and the corresponding direct brine releases are determined as shown in Table 4. The resultant CCDFs for direct brine releases to the accessible environment are then constructed (Sect. 11, Ref. 8) (Fig. 16). All the CCDFs fall below the boundary line specified in 191.13(a). Overall, the CCDFs tend to be farther from the boundary line and also more scattered than the CCDFs for cuttings and spallings (Figs. 6, 16, Ref. 11), with 51 out of 100 CCDFs being degenerate (i.e., having no nonzero releases) for replicate R1. However, the distribution is still stable across the three replicates (Fig. 17).

The primary determinants of the uncertainty in the CCDFs in Fig. 16 are the pressure and brine saturation conditions in the repository, with no direct brine releases taking place for low brine saturation (Figs. 8, 11, 13) and also no releases taking place for low pressures (Figs. 8, 11, 13). For undisturbed conditions, pressure is primarily influenced by factors related to gas generation (i.e., *WMICDFLG*, *WGRCOR*, *WASTWICK*, *HALPOR* and *ANHPRM* as indicated in Fig. 18 and Table 6 of Ref. 18); similarly, brine saturation is also primarily influenced by factors related to brine inflow and gas generation (i.e., *HALPOR*, *WMICDFLG*, *WGRCOR*, *WASTWICK*, and *ANHPRM* as indicated in Fig. 23 and Table 7 of Ref. 18). Subsequent to a drilling intrusion, pressure and saturation are determined primarily by borehole permeability (Figs. 32, 36, 37, Ref. 19).

To provide additional perspective, CCDFs for volume of brine released by direct brine release (i.e., the quantity obtained from Table 4 when C_{E0} and C_{E1} are set to 1) can also be constructed (Fig. 18). Similarly to cuttings and spallings (Figs. 9, 18, Ref. 11), the release of more than 10 m^3 of material (i.e., brine) over 10,000 yr is unlikely.

As was done for the cuttings and spallings CCDFs (Sects. 5, 10, Ref. 11), a sensitivity analysis based on stepwise regression analysis[32,33] with rank-transformed data[34] can be performed for the expected direct brine releases associated with each CCDF (Table 5). The dominant variables are residual brine saturation in waste (*WRBRNSAT*) and halite porosity (*HALPOR*), with the size of the release tending to decrease as *WRBRNSAT* increases and to increase as *HALPOR* increases. The negative effect for *WRBRNSAT* results from reducing the amount of brine that can take part in a direct brine release, and the positive effect for *HALPOR* results from increasing the amount of brine in the repository and also increasing the pressure in the repository under undisturbed conditions. Small positive effects are also indicated for logarithm of anhydrite permeability (*ANHPRM*), logarithm of bulk compressibility of brine pocket (*BPCOMP*), logarithm of halite permeability (*HALPRM*), initial pressure in brine pocket (*BPINTPRS*), and pointer variable for selection of brine pocket volume (*BPVOL*). However, the final regression models have R^2 values of only 0.49 and 0.50. Thus, these models are not very effective in accounting for the uncertainty in the analysis outcomes. This lack of resolution is due to the large number of sample elements that have no direct brine release. For example, the effects of *WRBRNSAT* and *HALPOR* can be readily seen in the scatterplots in Fig. 19; however, these effects tend to be obscured by the large number of zero releases. As a reminder, direct brine releases can only take place when the repository is at a pressure that exceeds 8 MPa.

The regressions in Table 5 included the solubilities of the individual elements as candidate independent variables (see Table 6 and also Table 1, Ref. 12). However, none of these solubilities were selected in the regression analysis. Basically, the uncertainty in whether or not a direct brine release takes place is swamping out the uncertainty induced by the solubilities when a release does take place. Also, borehole permeability (i.e., $k = 10^x$, $x =$ *BHPRM*) appears to have little effect on the expected release for direct brine release (Fig. 20); again, this is probably due to the dominant role played by the uncertainty in whether or not a direct brine release occurs at all.

The direct brine releases for individual futures were constructed with the assumption that each intrusion could result in a direct brine release (Table 4). However, releases after the first intrusion only occur if the pressure in the repository remains above 8 MPa (Fig. 13). The pressure in the repository subsequent to an intrusion is very dependent on the borehole permeability (Fig. 32, Ref. 19). In turn, this means that the occurrence of direct brine releases subsequent to an initial intrusion is also very dependent on borehole permeability (Fig. 13). In the present analysis, there is no variation in the permeability in a borehole above the repository for plugging patterns 2 and 3; specifically, all boreholes for a given LHS element are assumed to have the same permeability. As the repository rapidly drops below 8 MPa unless a borehole has a very low permeability, it is probably unreasonable to assume that the pressure in the repository after multiple intrusions has the same value as after a single intrusion. Rather, once a higher permeability borehole occurs, the pressure would drop below 8 MPa and no additional direct brine releases

would take place. Inclusion of this depressurization mechanism in the analysis would reduce the direct brine releases (Fig. 21). However, the differences between the CCDFs with no cutoff (Fig. 16) and the CCDFs with a two drilling intrusion cutoff (Fig. 21) are not large, which is consistent with the limited effect indicated for *BHPRM* in Fig. 20.

12. Discussion

The 1996 WIPP PA incorporated four direct release modes to the surface environment: cuttings, cavings, spallings, and direct brine release (DBR). The DBR is described in this article; the cuttings, cavings and spallings release modes are described in another article.[11] The DBRs were substantially smaller than the cuttings, cavings and spallings releases.[11] Further, like the spallings releases, DBRs had the potential to occur only when the pressure in the repository exceeded 8 MPa, which is the pressure exerted by a column of brine-saturated drilling fluid at the depth of the repository.[6] At lower pressures, brine and gas were assumed to be contained in the repository and so neither a spallings release nor a DBR could occur.

The 1996 WIPP PA also incorporated two distinct treatments of uncertainty: stochastic uncertainty (Sect. 3, Ref. 7; Ref. 8) and subjective uncertainty (Sect. 5, Ref. 7; Ref. 9), with stochastic uncertainty being characterized by a probability space (S_{st}, δ_{st}, p_{st}) and subjective uncertainty being characterized by a probability space (S_{su}, δ_{su}, p_{su}). Simple random sampling is used to propagate the effects of stochastic uncertainty through the analysis (Sect. 4, Ref. 7; Ref. 8), and Latin hypercube sampling is used to propagate the effects of subjective uncertainty through the analysis (Sect. 5, Ref. 7; Ref. 9). At a conceptual level, the treatment of stochastic and subjective uncertainty in the analysis of cuttings, cavings and spallings releases[11] is identical to the treatment of these uncertainties in the analysis of DBRs. Further, the same LHSs are used in the propagation of subjective uncertainty, and the same random samples are used in the construction of CCDFs arising from stochastic uncertainty. The use of the same samples permits results from different release modes (e.g., cuttings, cavings, spallings, DBR) to be combined to obtain results for total releases from the repository.[15]

Repository pressure is the primary determinant of whether or not a DBR occurs for a given drilling intrusion. The subjective, or state of knowledge, uncertainty in repository pressure at the time of an initial drilling intrusion is dominated by the extent to which microbial gas generation occurs, the rate at which corrosion of steel occurs, the extent to which capillary forces cause brine to be drawn into the waste, halite porosity and anhydrite permeability (Sects. 9, 11). Halite porosity and anhydrite permeability are important because they influence the amount of brine that will enter the repository and subsequently be involved in the corrosion of steel. Subsequent to a drilling intrusion, the uncertainty in repository pressure is dominated by borehole permeability. Given that repository pressure is above 8 MPa, brine saturation of the waste is the primary determinant of whether or not a DBR will occur, with no DBRs taking place for brine saturations below approximately 0.4. Prior to an initial drilling intrusion, the uncertainty in brine saturation in the repository is dominated by the consumption of brine by corrosion and the

extent to which brine inflow to the repository occurs. Subsequent to a drilling intrusion, brine saturation in the repository is dominated by brine flow in the intruding borehole; however, repository pressure is usually not high enough for second and subsequent drilling intrusions to result in DBRs.

For a given DBR, the uncertainty in the radionuclide content of the release is determined by the uncertainty in radionuclide solubilities (Sect. 10). However, the effects of uncertainty in radionuclide solubilities tends to be overwhelmed by the greater effect of the uncertainty in whether or not a DBR event occurs.

Even when the effects of subjective uncertainty are taken into account, the CCDFs for DBR fall substantially below and to the left of the EPA boundary line for releases to the accessible environment specified in 40 CFR 191 (Fig. 16). Further, although there is substantial uncertainty in the location of the CCDF for DBR, the replicated LHSs indicate that the sample sizes in use (i.e., 100 for the individual replicates and 300 for the 3 pooled replicates) are adequate for assessing compliance with the boundary line for releases to the accessible environment. Specifically, the numerical uncertainty in the estimate of the distribution of CCDFs is small relative to the separation between the distribution and the boundary line. In the preceding sentence, numerical uncertainty refers to the uncertainty that enters the analysis due to the use of a sampling (i.e., Monte Carlo) procedure to estimate an integral over the probability space for subjective uncertainty.

The CCDFs for DBRs are substantially below and to the left of the CCDFs for cuttings and cavings (Fig. 6, Ref. 11), with the result that DBR does not contribute significantly to the total release to the accessible environment and thus to assessing compliance with the boundary line specified in 40 CFR 191.[15] As for the spallings CCDFs, the DBR CCDFs could be moved farther to the right by including the depressurization effects of initial drilling intrusions through the operations and experimental areas (Sect. 11, Ref. 11); however, the inclusion of this effect would have little impact on assessing compliance with 40 CFR 191 due to the dominant role played by the cuttings and cavings releases.

Acknowledgment

Work performed for Sandia National Laboratories (SNL), which is a multiprogram laboratory operated by Sandia Corporation, a Lockheed Martin Company, for the United States Department of Energy under contract DE-AC04-94AL85000. Review provided at SNL by M. Chavez, C. Crawford and M.S. Tierney. Editorial support provided by L. Harrison, T. Allen and H. Radke of Tech Reps, Inc.

References

1. U.S. Environmental Protection Agency, 40 CFR Part 191: Environmental Standards for the Management and Disposal of Spent Nuclear Fuel, High-Level and Transuranic Radioactive Wastes; Final Rule, *Federal Register*, 1985, **50**, 38066-38089.

2. U.S. Environmental Protection Agency, 40 CFR Part 191: Environmental Radiation Protection Standards for the Management and Disposal of Spent Nuclear Fuel, High-Level and Transuranic Radioactive Wastes; Final Rule, *Federal Register*, 1993, **58**, 66398-66416.

3. U.S. Environmental Protection Agency, 40 CFR Part 194: Criteria for the Certification and Re-Certification of the Waste Isolation Pilot Plant's Compliance With the 40 CFR Part 191 Disposal Regulations; Final Rule, *Federal Register*, 1996, **61**, 5224-5245.

4. Howard, B. et al., Regulatory Requirements Placed on the Waste Isolation Pilot Plant, *Reliability Engineering and System Safety* (in this issue).

5. U.S. Department of Energy, *Title 40 CFR Part 191 Compliance Certification Application for the Waste Isolation Pilot Plant*, DOE/CAO-1996-2184, Volumes I-XXI, U.S. Department of Energy, Carlsbad Area Office, Carlsbad, NM, 1996.

6. Stoelzel, D.M. & O'Brien, D.G., Analysis Package for the BRAGFLO Direct Release Calculations (Task 4) of the Performance Assessment AnalysesSupporting the Compliance Certification Application, Sandia WIPP Central Files WPO # 40520, Sandia National Laboratories, Albuquerque, NM, 1996.

7. Helton, J.C., Anderson, D.R., Jow, H.-N., Marietta, M.G., & Basabilvazo, G., Conceptual Structure of the 1996 Performance Assessment for the Waste Isolation Pilot Plant, *Reliability Engineering and System Safety* (in this issue).

8. Helton, J.C., Davis, F.J., & Johnson, J.D., Characterization of Stochastic Uncertainty in the 1996 Performance Assessment for the Waste Isolation Pilot Plant, *Reliability Engineering and System Safety* (in this issue).

9. Helton, J.C., Martell, M.-A., & Tierney, M.S., Characterization of Subjective Uncertainty in the 1996 Performance Assessment for the Waste Isolation Pilot Plant, *Reliability Engineering and System Safety* (in this issue).

10. Vaughn, P., Bean, J.E., Helton, J.C., Lord, M.E., MacKinnon, R.J., & Schreiber, J.D., Representation of Two-Phase Flow in the Vicinity of the Repository in the 1996 Performance Assessment for the Waste Isolation Pilot Plant, *Reliability Engineering and System Safety* (in this issue).

11. Berglund, J.W., Garner, J.W., Helton, J.C., Johnson, J.D., & Smith, L.N., Direct Releases to the Surface and Associated Complementary Cumulative Distribution Functions in the 1996 Performance Assessment for the Waste Isolation Pilot Plant: Cuttings, Cavings and Spallings, *Reliability Engineering and System Safety* (in this issue).

12. Stockman, C.T., Garner, J.W., Helton, J.C., Johnson, J. D., Shinta, A., & Smith, L.N., Radionuclide Transport in the Vicinity of the Repository and Associated Complementary Cumulative Distribution Functions in the 1996 Performance Assessment for the Waste Isolation Pilot Plant, *Reliability Engineering and System Safety* (in this issue).

13. Ramsey, J.L., Blaine, R., Garner, J.W., Helton, J.C., Johnson, J.D., Smith, L.N., & Wallace, M., Radionuclide and Colloid Transport in the Culebra Dolomite and Associated Complementary Cumulative Distribution Functions in the 1996 Performance Assessment for the Waste Isolation Pilot Plant, *Reliability Engineering and System Safety* (in this issue).

14. Poettmann, F.H. & Carpenter, P.G., Multiphase Flow of Gas, Oil, and Water through Vertical Flow Strings with Application to the Design of Gas-Lift Installations, *Drilling and Production Practice*, American Petroleum Institute, Washington, DC, 1952, 257-317.

15. Helton, J.C., Anderson, D.R., Basabilvazo, G., Jow, H.-N., & Marietta, M.G., Summary Discussion of the 1996 Performance Assessment for the Waste Isolation Pilot Plant, *Reliability Engineering and System Safety* (in this issue).

16. McKay, M.D., Beckman, R.J., & Conover, W.J., A Comparison of Three Methods for Selecting Values of Input Variables in the Analysis of Output from a Computer Code, *Technometrics*, 1979, **21** (2), 239-245.

17. Helton, J.C., Uncertainty and Sensitivity Analysis Techniques for Use in Performance Assessment for Radioactive Waste Disposal, *Reliability Engineering and System Safety*, 1993, **42** (2-3), 327-367.

18. Helton, J.C., Bean, J.E., Economy, K., Garner, J.W., MacKinnon, R.J., Miller, J., Schreiber, J.D., & Vaughn, P., Uncertainty and Sensitivity Analysis for Two-Phase Flow in the Vicinity of the Repository in the 1996 Performance Assessment for the Waste Isolation Pilot Plant: Undisturbed Conditions, *Reliability Engineering and System Safety* (in this issue).

19. Helton, J.C., Bean, J.E., Economy, K., Garner, J.W., MacKinnon, R.J., Miller, J., Schreiber, J.D., & Vaughn, P., Uncertainty and Sensitivity Analysis for Two-Phase Flow in the Vicinity of the Repository in the 1996 Performance Assessment for the Waste Isolation Pilot Plant: Disturbed Conditions, *Reliability Engineering and System Safety* (in this issue).

20. Helton, J.C., Bean, J.E., Berglund, J.W., Davis, F.J., Economy, K., Garner, J.W., Johnson, J.D., MacKinnon, R.J., Miller, J., O'Brien, D.G., Ramsey, J.L., Schreiber, J.D., Shinta, A., Smith, L.N., Stoelzel, D.M., Stockman, C., & Vaughn, P., *Uncertainty and Sensitivity Analysis Results Obtained in the 1996 Performance Assessment for the Waste Isolation Pilot Plant*, SAND98-0365, Sandia National Laboratories, Albuquerque, NM, 1998.

21. Mattax, C.C. & Dalton, R. L., *Reservoir Simulation*, SPE Monograph 13. Henry L. Doherty Memorial Fund of AIME, Society of Petroleum Engineers, Inc., Richardson, TX, 1990.

22. Williamson, A.S. & Chappelear, J.E., Representing Wells in Numerical Reservoir Simulation: Part 1 - Theory. Representing Wells in Numerical Reservoir Simulation: Part 2 - Implementation, *Society of Petroleum Engineers Journal*, 1981, **21** (3), 323-338.

23. Kaufmann, D.W., *Sodium Chloride, The Production and Properties of Salt and Brine*, ACS Monograph 145. American Chemical Society, Washington, DC; Reinhold Pub Corp, New York, 1960.

24. Gatlin, C., *Petroleum Engineering: Drilling and Well Completions*, Prentice Hall, Inc., Englewood Cliffs, NJ, 1960.

25. Lee, J., *Well Testing*, Society of Petroleum Engineers of AIME, New York, NY, 1982.

26. Brill, J.P. & Beggs, H.D., *Two-Phase Flow in Pipes*, 5th ed., first printing. University of Tulsa, Tulsa, OK, 1986.

27. Welchon, J.K., Bertuzzi, A.F., & Poettmann, F.H., Chapter 31 Wellbore Hydraulics, *Petroleum Production Handbook, Volume 2*, Eds. T.C. Frick and R.W. Taylor, Society of Petroleum Engineers of AIME, Dallas, TX, 1962, pp. 31-1 to 31-36.

28. Ely, J.F. & Huber, M.L., *NIST Thermophysical Properties of Hydrocarbon Mixtures Database (SUPERTRAPP), Version 1.0, User's Guide*. Gaithersburg, MD: U.S. Department of Commerce, National Institute of Standards and Technology, Standard Reference Data Program, Sandia WIPP Central Files WPO # 42589, Sandia National Laboratories, Albuquerque, NM, 1992.

29. Prasuhn, A.L., *Fundamentals of Fluid Mechanics*, Prentice Hall, Inc., Englewood Cliffs, NJ, 1980.

30. WIPP PA, *BRAGFLO, Version 4.00, User's Manual*, Sandia WIPP Central Files WPO # 30703, Sandia National Laboratories, Albuquerque, NM, 1996.

31. Stockman, C., Shinta, A., & Garner, J.W., Analysis Package for the Salado Transport Calculations (Task 2) of the Performance Assessment Analysis Supporting the Compliance Certification Application, Sandia WIPP Central Files WPO # 40515, Sandia National Laboratories, Albuquerque, NM, 1996.

32. Iman, R.L, Davenport, J.M., Frost, E.L., & Shortencarier, M.J., *Stepwise Regression with PRESS and Rank Regression (Program User's Guide)*, SAND79-1472, Sandia National Laboratories, Albuquerque, NM, 1980.

33. WIPP PA (Performance Assessment), *STEPWISE, Version 2.20, User's Manual [Document Version 1]*, Sandia WIPP Central Files WPO # 27768, Sandia National Laboratories, Albuquerque, NM, 1995.

34. Iman, R.L., & Conover, W.J., The Use of the Rank Transform in Regression, *Technometrics*, 1979, **21** (4), 499-509.

Figure Captions

Fig. 1. Direct brine release (BRAGFLO_DBR) mesh.

Fig. 2. Representation of coupling between grids in Fig. 1 of Ref. 10 and Fig. 1 to obtain initial conditions for direct brine release calculation at each intrusion time.

Fig. 3. Borehole representation used for Poettmann-Carpenter correlation.

Fig. 4. Flowing bottom hole pressure (FBHP) (i.e., p_{wf} in Eq. (25)) as a function of brine well index (i.e., J_b in Eq. (8)) and panel pressure for a system with only mobile brine (i.e., $k_{rg} = 0$) (Fig. B1, Ref. 6).

Fig. 5. Flowing bottom hole pressure (FBHP) (i.e., p_{wf} in Eq. (25)) as a function of relative permeabilities and panel pressure for a brine dominated system (i.e., $\log (k_{rg}/k_{rb}) \leq 0$) (Fig. B2, Ref. 6).

Fig. 6. Flowing bottom hole pressure (FBHP) (i.e., p_{wf} in Eq. (25)) as a function of relative permeabilities and panel pressure for a gas dominated system (i.e., $\log (k_{rg}/k_{rb}) > 0$) (Fig. B3, Ref. 6).

Fig. 7. Distribution of brine release and normalized release due to direct brine release for a single drilling intrusion into a previously unintruded repository.

Fig. 8. Scatterplots for volume of brine removed from repository due to direct brine release resulting from a single drilling intrusion at 5000 yr into a previously unintruded repository that passes through CH-TRU waste in a lower waste panel versus brine saturation (*WAS_SATB*) and pressure (*WAS_PRES*) in that panel.

Fig. 9. Scatterplots for brine saturation (*WAS_SATB*) versus pressure (*WAS_PRES*) in lower waste panels of undisturbed repository at 5000 yr.

Fig. 10. Scatterplot for normalized release from repository due to direct brine release resulting from a single drilling intrusion at 10,000 yr into a previously unintruded repository that passes through CH-TRU waste in a lower waste panel versus radionuclide concentration at 10,000 yr.

Fig. 11. Three dimensional scatterplots for volume of brine removed due to direct brine release resulting from a single drilling intrusion at 5000 yr into a previously unintruded repository that passes through CH-TRU waste in a lower waste panel, brine saturation (*WAS_SATB*) and pressure (*WAS_PRES*).

Fig. 12. Distribution of brine release and normalized release due to direct brine release for the second drilling intrusion into CH-TRU waste after an initial intrusion at 1000 yr. Similar results were obtained for initial intrusions at 350 yr (Figs. 10.1.6, 10.1.7, Ref. 20).

Fig. 13. Scatterplots for volume of brine removed from repository due to direct brine release resulting from second drilling intrusion into CH-TRU waste in same waste panel as an initial E1 intrusion versus brine saturation (*WAS_SATB*), pressure (*WAS_PRES*) and logarithm of borehole permeability (*BHPRM*).

Fig. 14. Radionuclide concentration (EPA units/m^3) in repository brine with MgO backfill.

Fig. 15. Radionuclide concentration (EPA units/m^3) in repository brine without MgO backfill.

Fig. 16. Distribution of CCDFs for normalized release to accessible environment over 10,000 yr due to direct brine release: (16a) CCDFs for replicate R1, and (16b) mean and percentile curves obtained by pooling replicates R1, R2 and R3.

Fig. 17. Outcome of replicated sampling for distribution of CCDFs for normalized release to the accessible environment over 10,000 yr due to direct brine release: (17a) mean and percentile curves for individual replicates, and (17b) confidence intervals (CIs) on mean curve obtained from the three replicates.

Fig. 18. Distribution of CCDFs for volume of brine removed to accessible environment over 10,000 yr due to direct brine release: (18a) CCDFs for replicate R1, and (18b) mean and percentile curves obtained by pooling replicates R1, R2 and R3.

Fig. 19. Scatterplots for expected normalized releases associated with individual CCDFs for direct brine release versus *WRBRNSAT* and *HALPOR*.

Fig. 20. Scatterplot for expected normalized releases associated with individual CCDFs for direct brine release versus *BHPRM*.

Fig. 21. Distribution of CCDFs obtained with replicate R1 for normalized release to accessible environment over 10,000 yr due to direct brine release with the assumption that direct brine releases will only take place for the first two drilling intrusions into the repository.

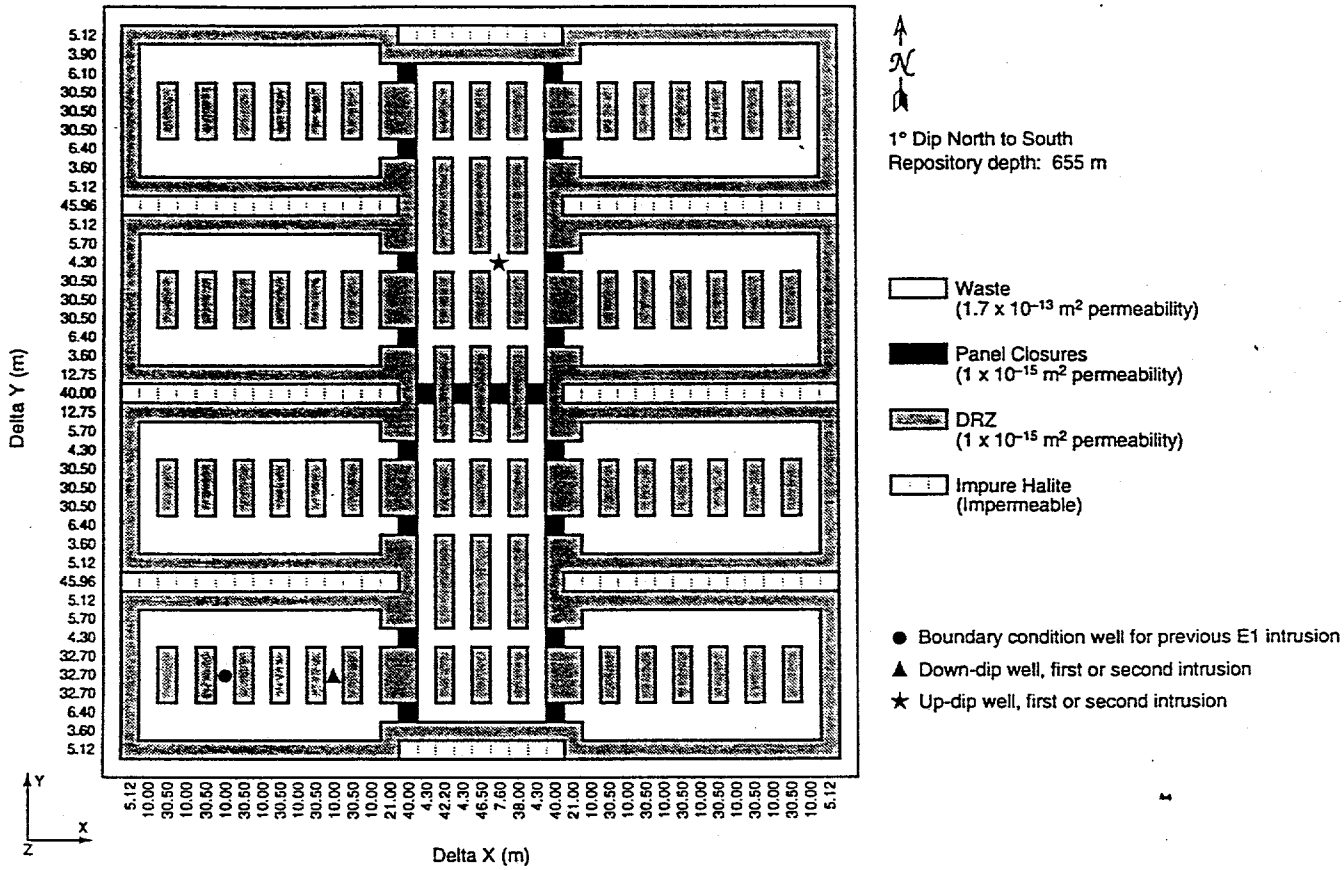

Note: Model cells are not to scale. The actual dimensions of the grid blocks are indicated along the edge of the diagram.

TRI-6342-5432-3

Fig. 1. Direct brine release (BRAGFLO_DBR) mesh.

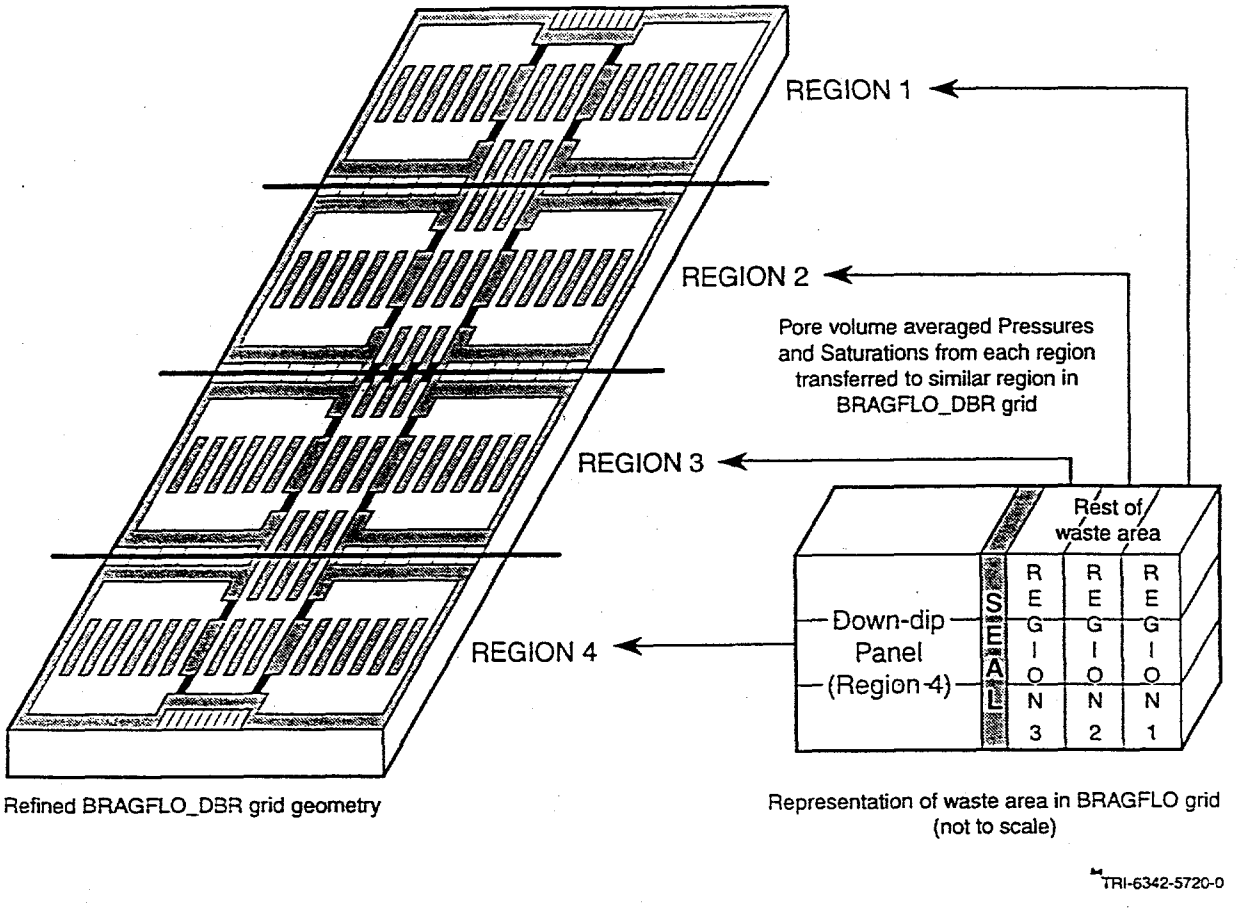

Fig. 2. Representation of coupling between grids in Fig. 1 of Ref. 10 and Fig. 1 to obtain initial conditions for direct brine release calculation at each intrusion time.

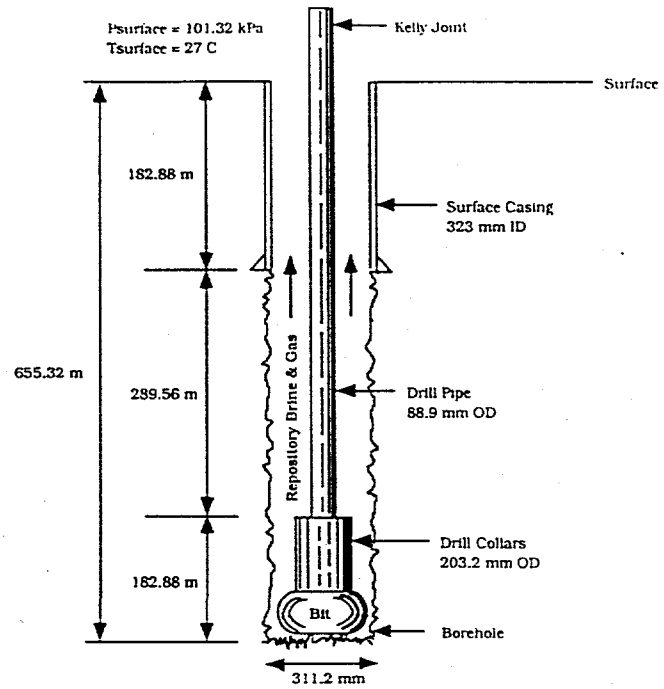

Fig. 3. Borehole representation used for Poettmann-Carpenter correlation.

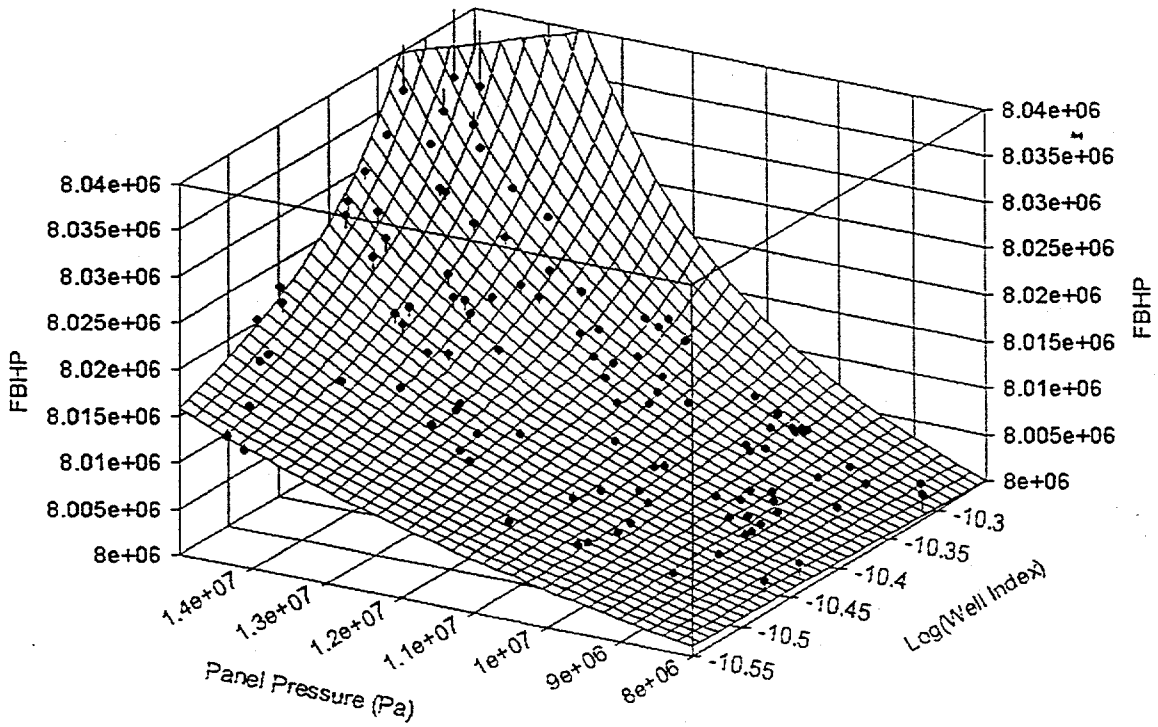

Fig. 4. Flowing bottom hole pressure (FBHP) (i.e., p_{wf} in Eq. (25)) as a function of brine well index (i.e., J_b in Eq. (8)) and panel pressure for a system with only mobile brine (i.e., $k_{rg} = 0$) (Fig. B1, Ref. 6).

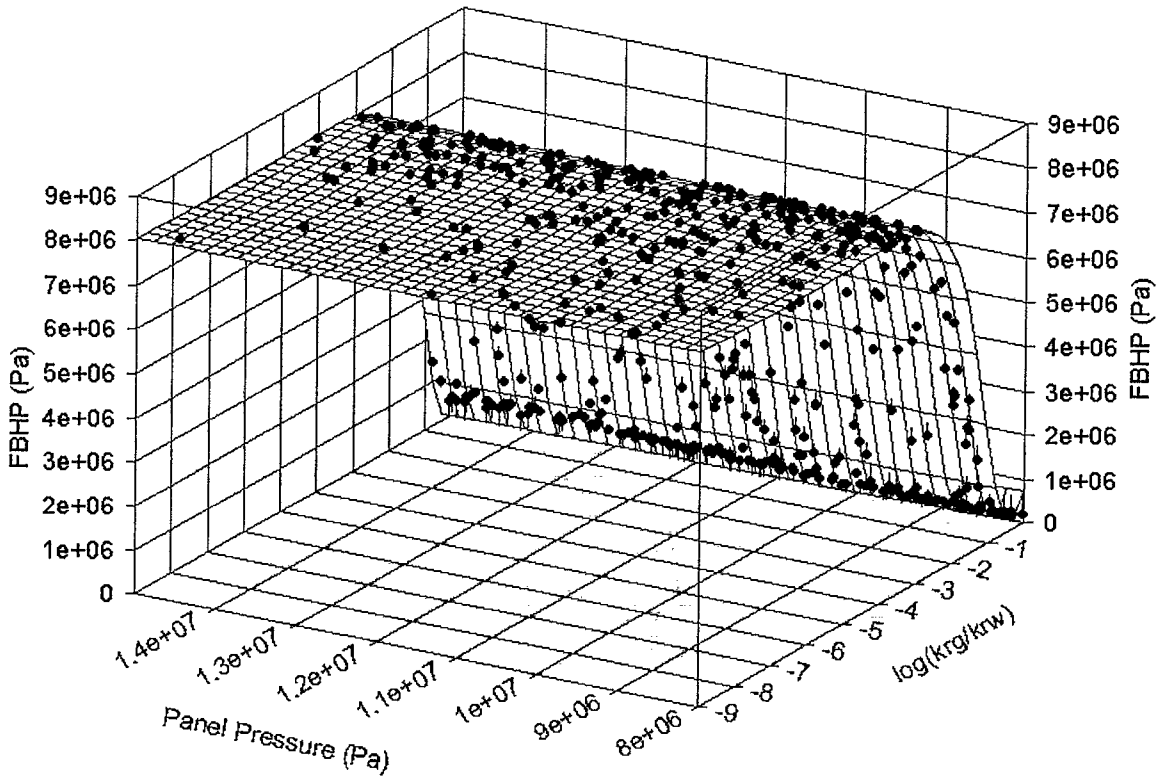

Fig. 5. Flowing bottom hole pressure (FBHP) (i.e., p_{wf} in Eq. (25)) as a function of relative permeabilities and panel pressure for a brine dominated system (i.e., log $(k_{rg}/k_{rb}) \leq 0$) (Fig. B2, Ref. 6).

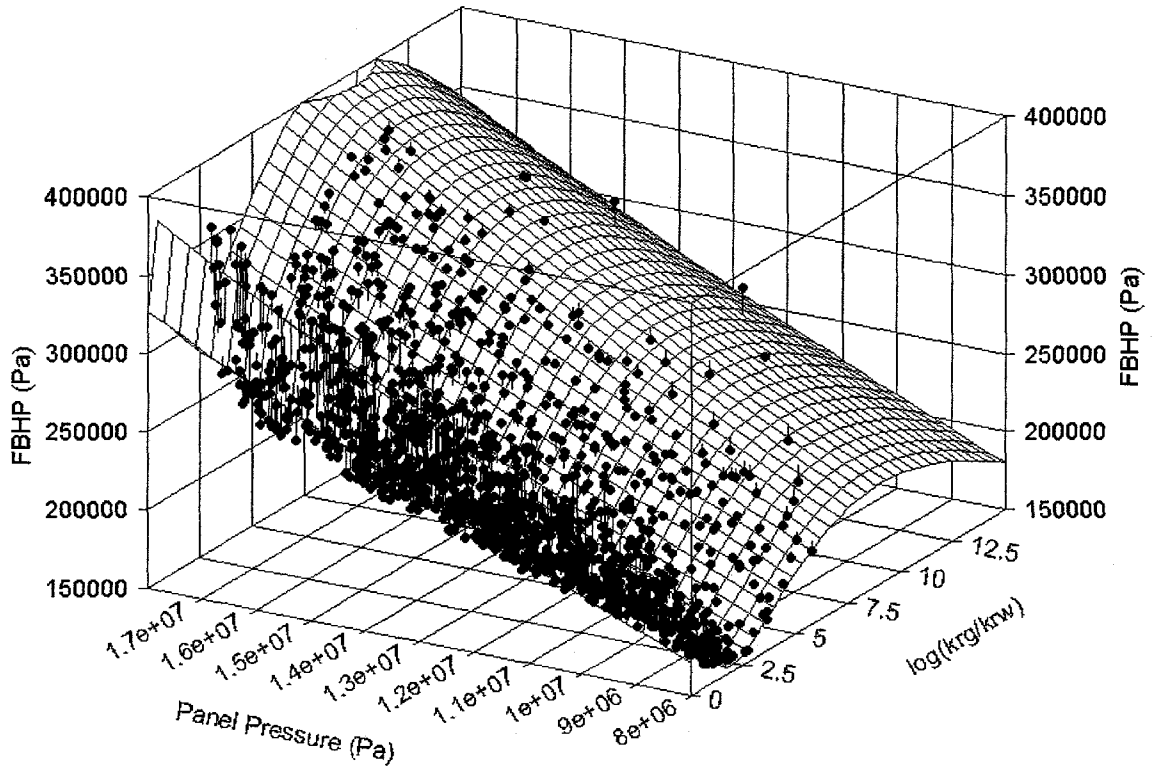

Fig. 6. Flowing bottom hole pressure (FBHP) (i.e., p_{wf} in Eq. (25)) as a function of relative permeabilities and panel pressure for a gas dominated system (i.e., log $(k_{rg}/k_{rb}) > 0$) (Fig. B3, Ref. 6).

Fig. 7. Distribution of brine release and normalized release due to direct brine release for a single drilling intrusion into a previously unintruded repository.

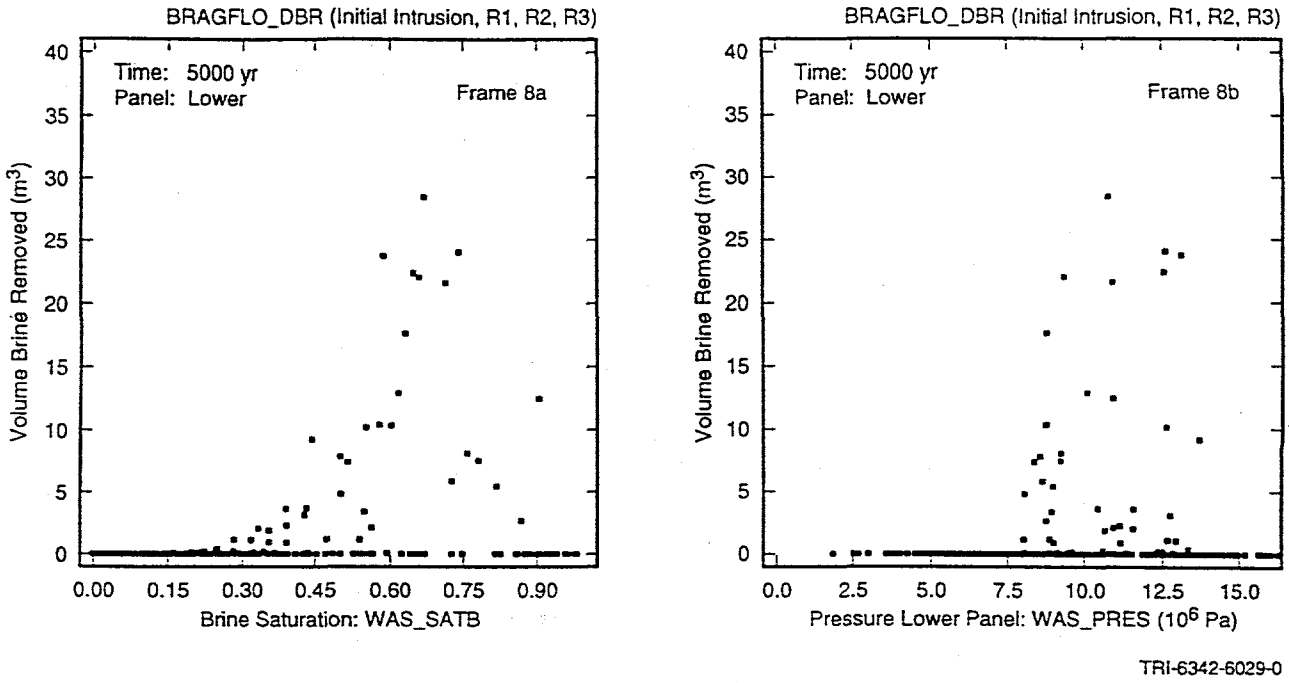

Fig. 8. Scatterplots for volume of brine removed from repository due to direct brine release resulting from a single drilling intrusion at 5000 yr into a previously unintruded repository that passes through CH-TRU waste in a lower waste panel versus brine saturation (*WAS_SATB*) and pressure (*WAS_PRES*) in that panel.

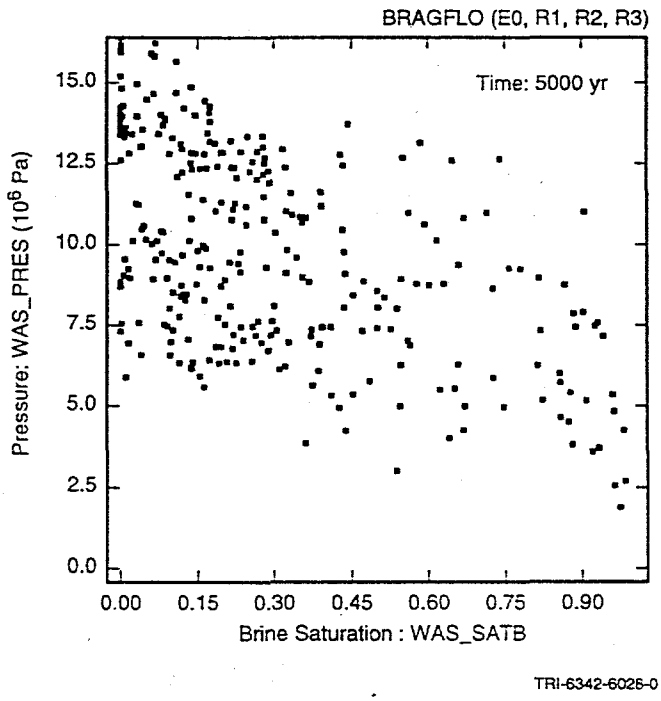

Fig. 9. Scatterplots for brine saturation (*WAS_SATB*) versus pressure (*WAS_PRES*) in lower waste panels of undisturbed repository at 5000 yr.

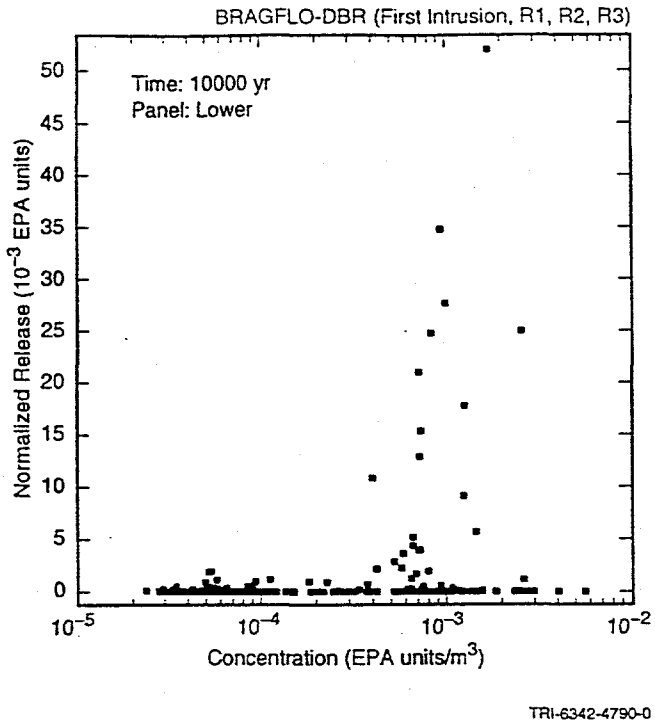

Fig. 10. Scatterplot for normalized release from repository due to direct brine release resulting from a single drilling intrusion at 10,000 yr into a previously unintruded repository that passes through CH-TRU waste in a lower waste panel versus radionuclide concentration at 10,000 yr.

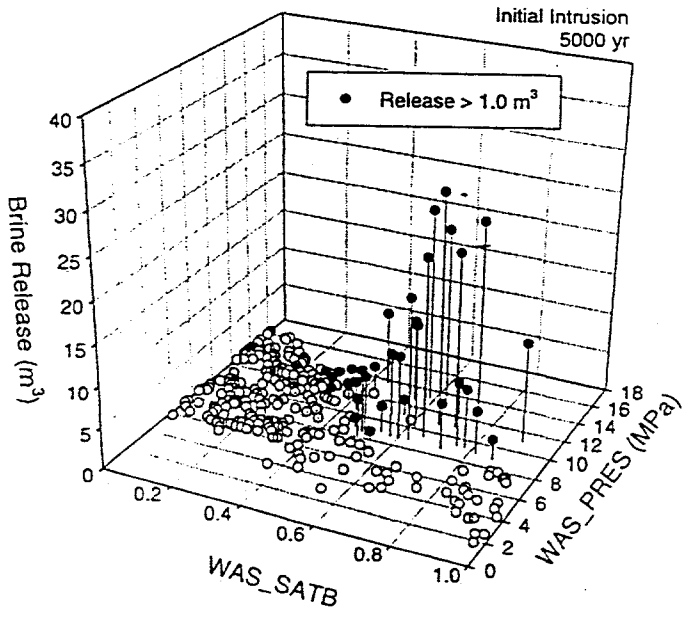

Fig. 11. Three dimensional scatterplots for volume of brine removed due to direct brine release resulting from a single drilling intrusion at 5000 yr into a previously unintruded repository that passes through CH-TRU waste in a lower waste panel, brine saturation (*WAS_SATB*) and pressure (*WAS_PRES*).

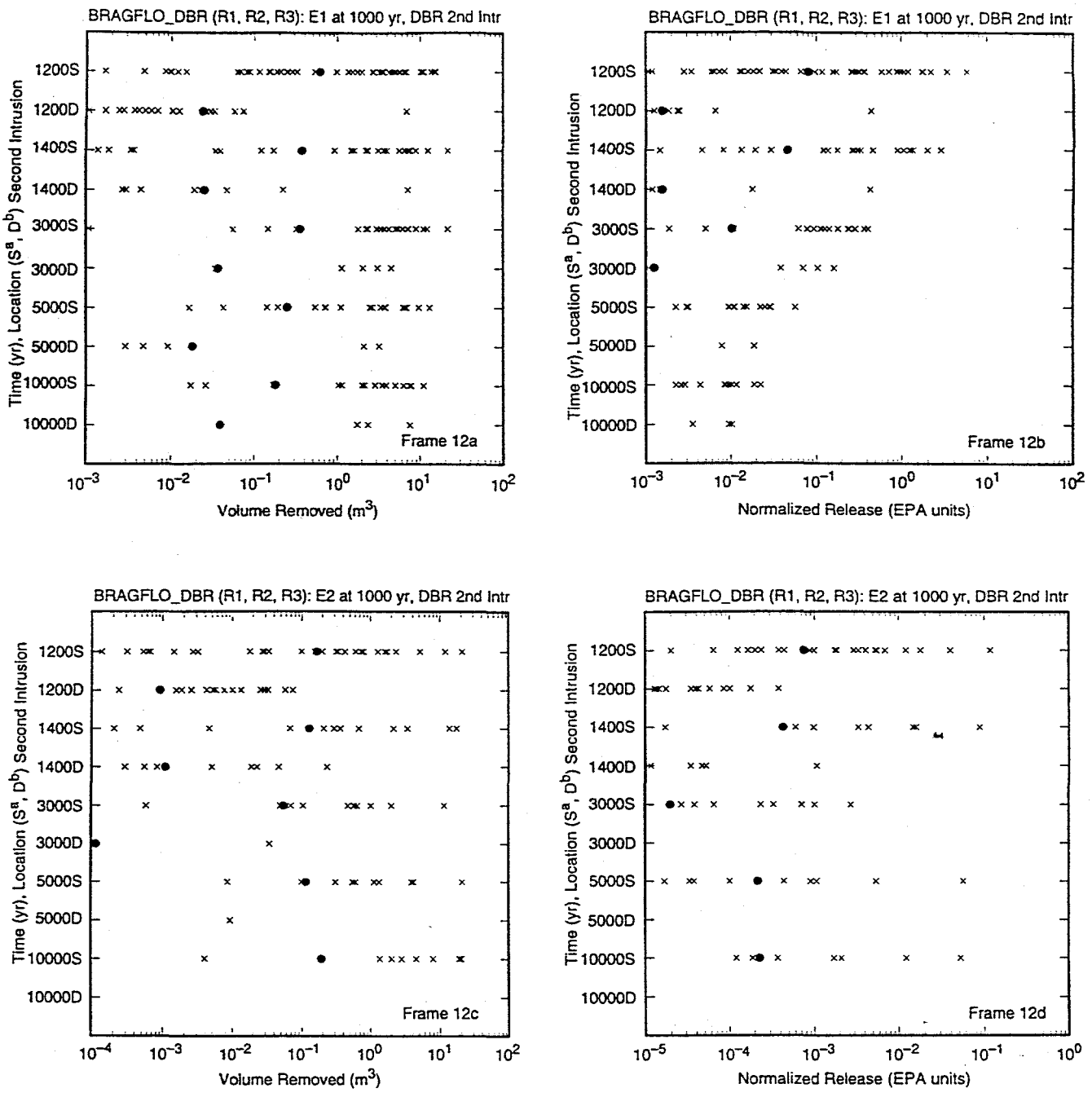

[a]S Signifies Second Intrusion Occurs in Same (S) Waste Panel as First Intrusion

[b]D Signifies Second Intrusion Occurs in Different (D) Waste Panel than First Intrusion

TRI-6342-6030-0

Fig. 12. Distribution of brine release and normalized release due to direct brine release for the second drilling intrusion into CH-TRU waste after an initial intrusion at 1000 yr. Similar results were obtained for initial intrusions at 350 yr (Figs. 10.1.6, 10.1.7, Ref. 20).

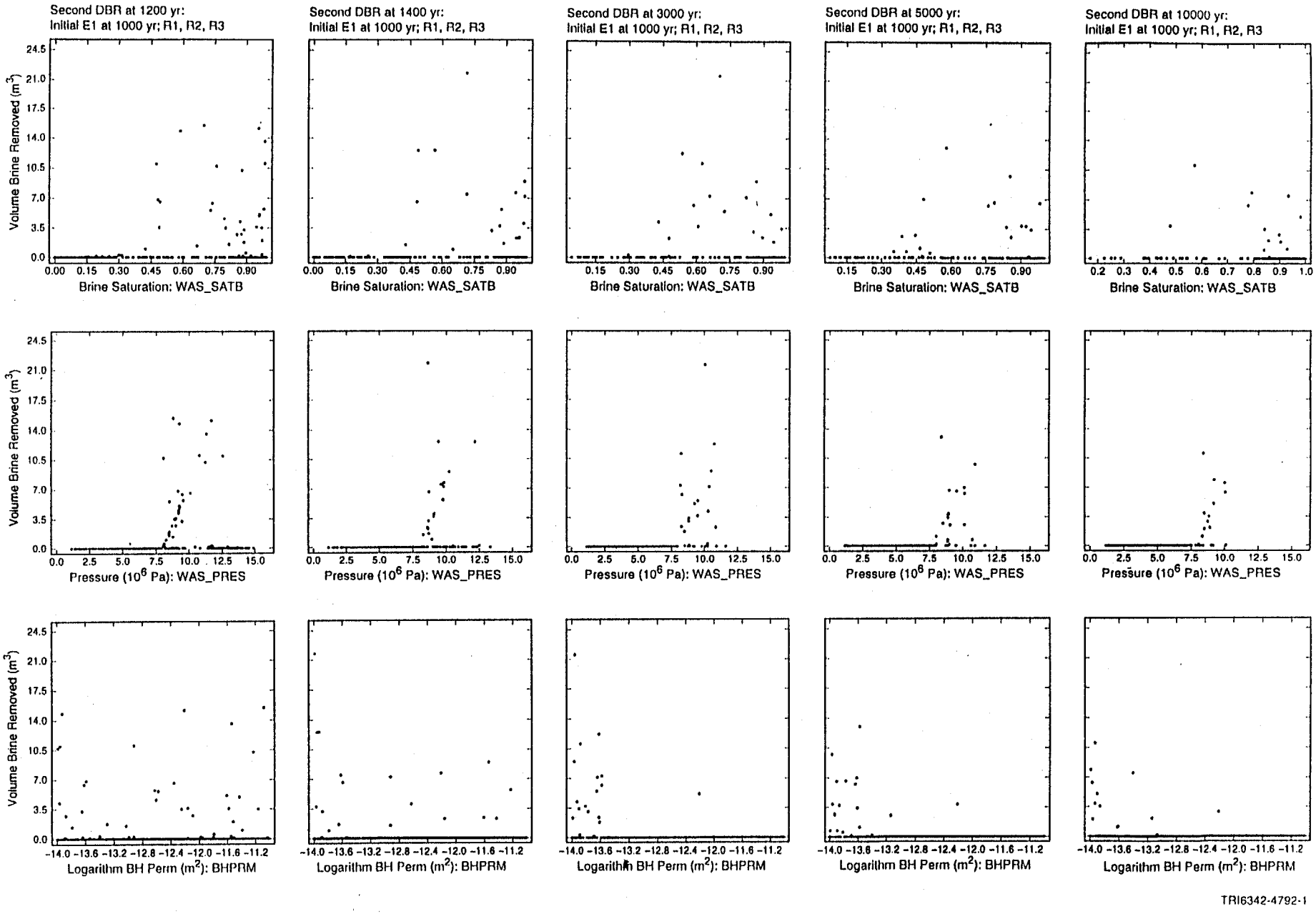

Fig. 13. Scatterplots for volume of brine removed from repository due to direct brine release resulting from second drilling intrusion into CH-TRU waste in same waste panel as an initial E1 intrusion versus brine saturation (*WAS_SATB*), pressure (*WAS_PRES*) and logarithm of borehole permeability (*BHPRM*).

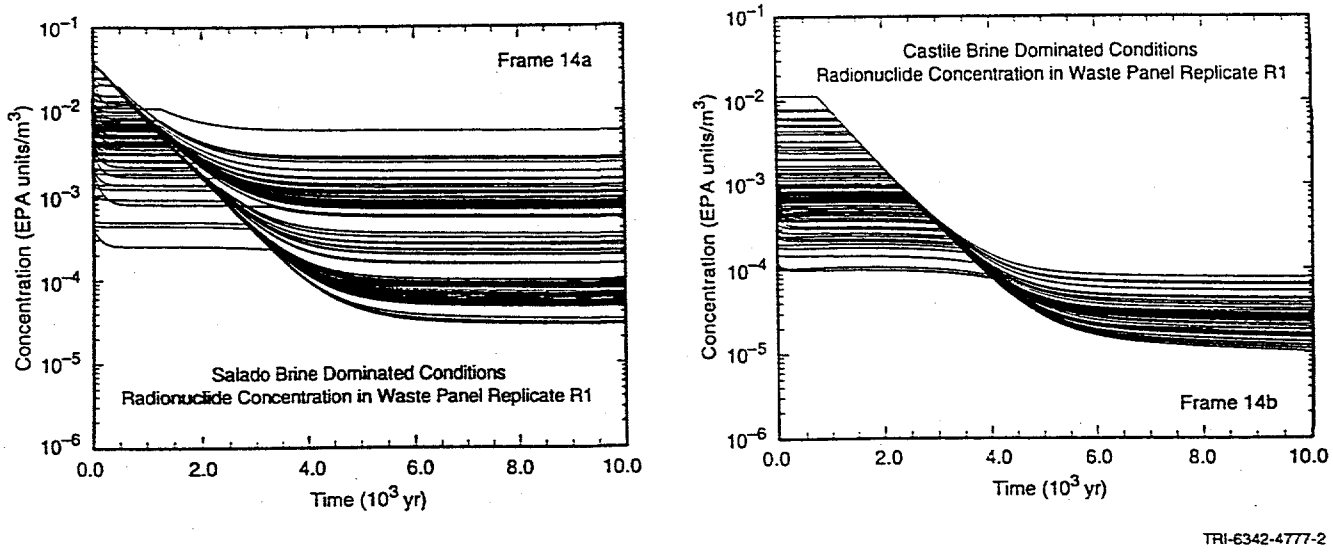

Fig. 14. Radionuclide concentration (EPA units/m^3) in repository brine with MgO backfill.

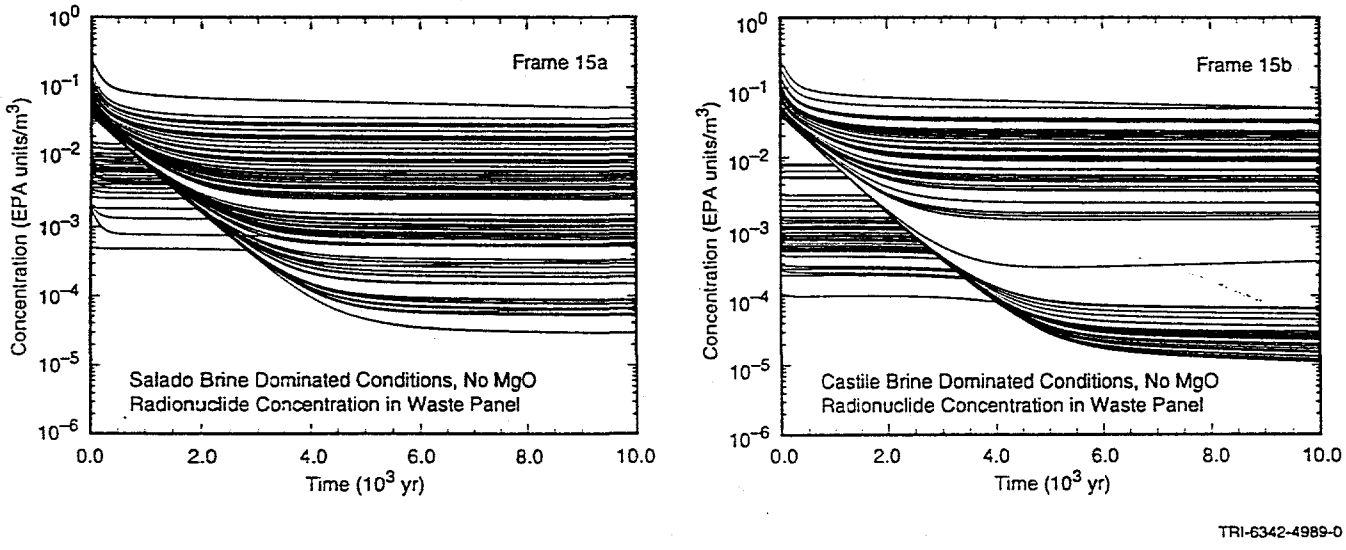

Fig. 15. Radionuclide concentration (EPA units/m^3) in repository brine without MgO backfill.

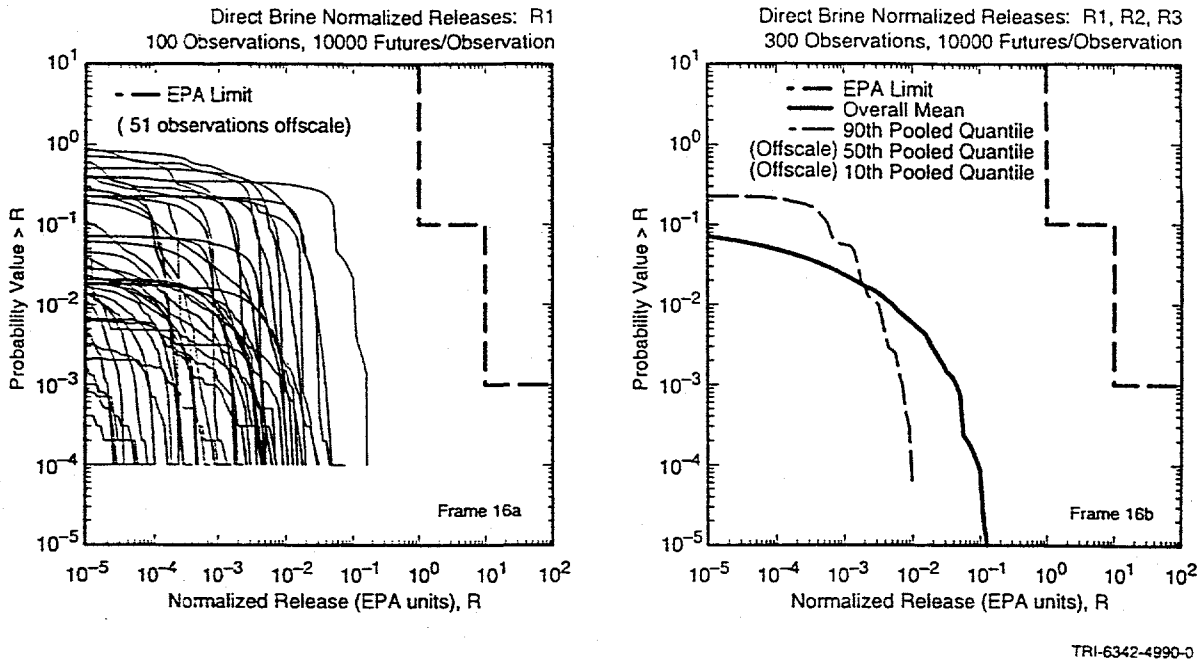

Fig. 16. Distribution of CCDFs for normalized release to accessible environment over 10,000 yr due to direct brine release: (16a) CCDFs for replicate R1, and (16b) mean and percentile curves obtained by pooling replicates R1, R2 and R3.

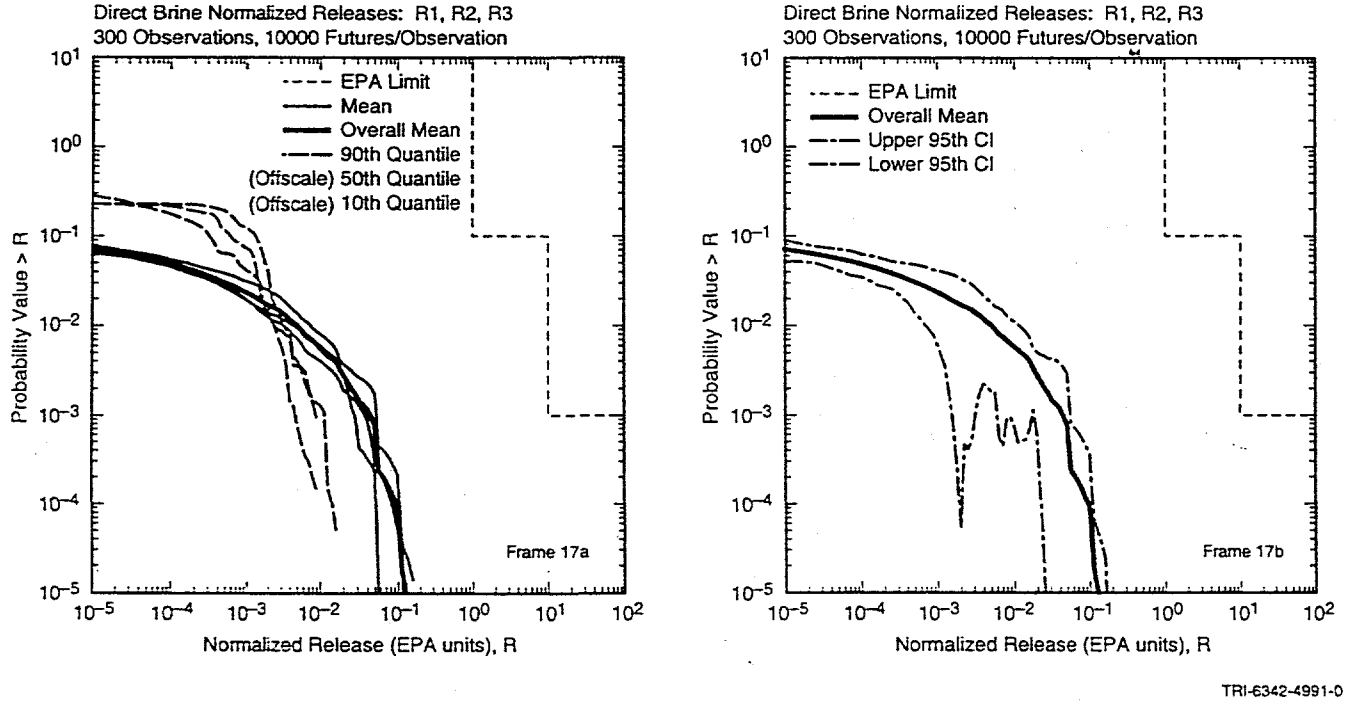

Fig. 17. Outcome of replicated sampling for distribution of CCDFs for normalized release to the accessible environment over 10,000 yr due to direct brine release: (17a) mean and percentile curves for individual replicates, and (17b) confidence intervals (CIs) on mean curve obtained from the three replicates.

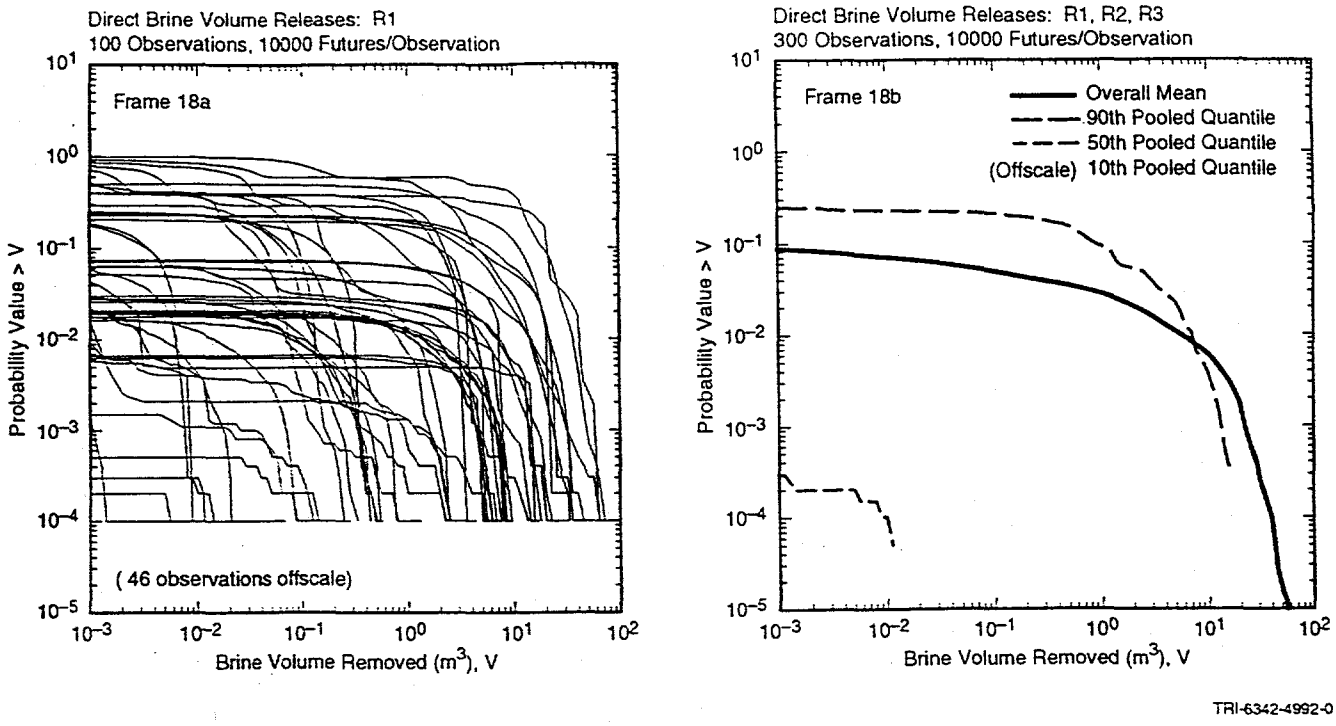

Fig. 18. Distribution of CCDFs for volume of brine removed to accessible environment over 10,000 yr due to direct brine release: (18a) CCDFs for replicate R1, and (18b) mean and percentile curves obtained by pooling replicates R1, R2 and R3.

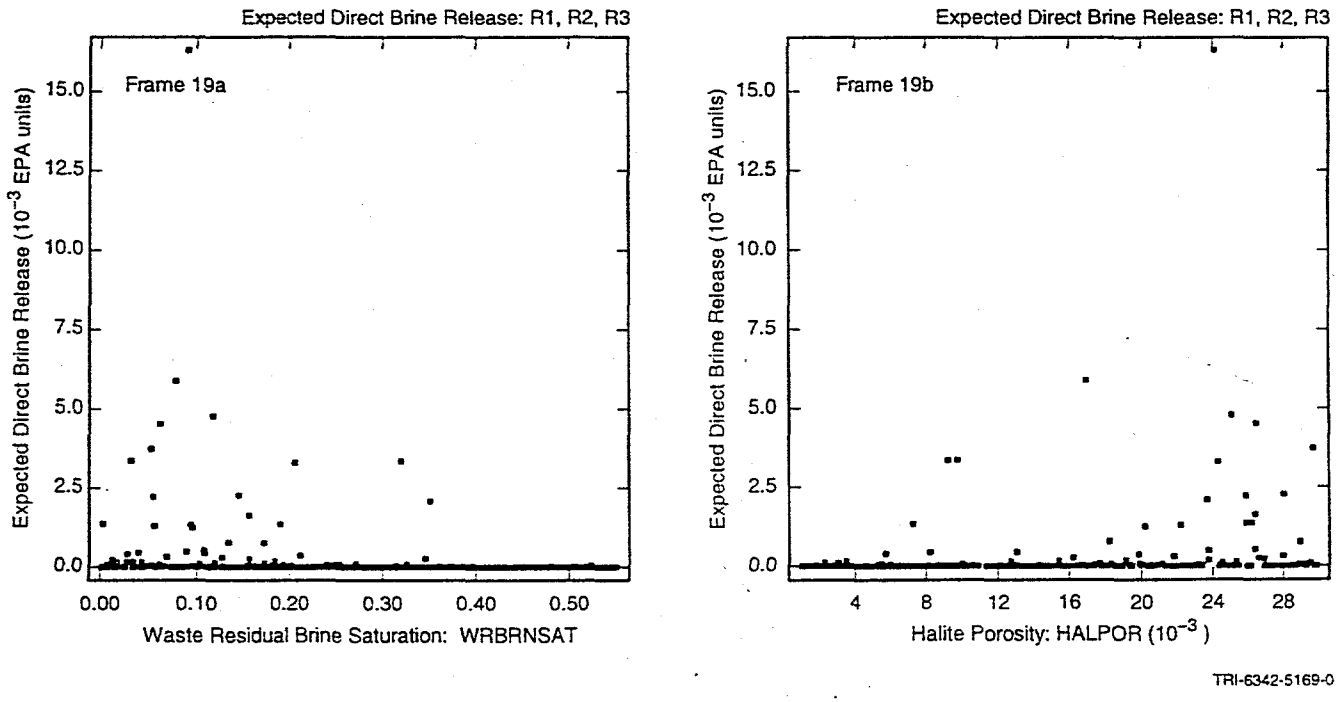

Fig. 19. Scatterplots for expected normalized releases associated with individual CCDFs for direct brine release versus *WRBRNSAT* and *HALPOR*.

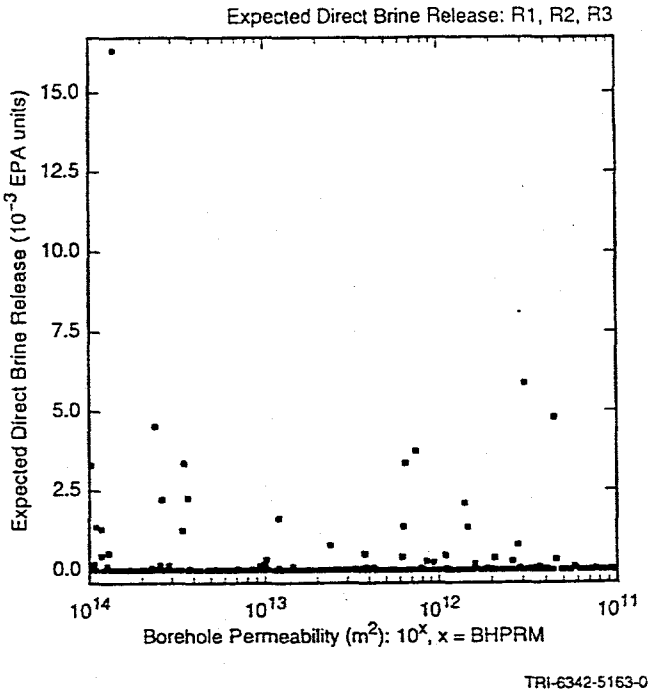

Fig. 20. Scatterplot for expected normalized releases associated with individual CCDFs for direct brine release versus *BHPRM*.

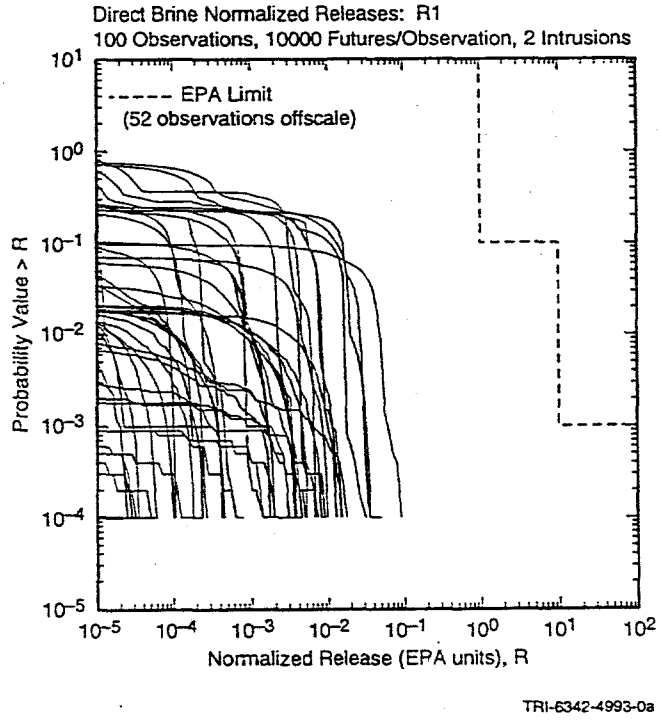

Fig. 21. Distribution of CCDFs obtained with replicate R1 for normalized release to accessible environment over 10,000 yr due to direct brine release with the assumption that direct brine releases will only take place for the first two drilling intrusions into the repository.

Table 1. Initial Definition (i.e., Initial Value Conditions) for Brine Pressure *pb* (*x*, *y*, 0), Gas Saturation *Sg* (*x*, *y*, 0) and Porosity ϕ (*x*, *y*, 0) for Computational Grid in Fig. 1, where (*x*, *y*) Designates a Point in the Grid and t = 0 yr Corresponds to Time at which Drilling Intrusion Occurs

Values for $p_b(x, y, 0)$ and $S_g(x, y, 0)$

$$p_b(x, y, 0) = \int_R \tilde{p}_b(\tilde{x}, \tilde{y}, t_{int}) dV \Big/ \int_R dV$$

$$S_g(x, y, 0) = \int_R \tilde{S}_g(\tilde{x}, \tilde{y}, t_{int}) dV \Big/ \int_R dV$$

where $\tilde{p}_b$ and $\tilde{S}_g$ denote solutions to Eqs. (2) - (7) of Ref. 10, $\tilde{x}$ and $\tilde{y}$ denote the variables of integration, t_{int} is the time at which the drilling intrusion occurs (Note: t_{int} defines a time in the solution of Eqs. (2) - (7) of Ref. 10; t = 0 defines the start time for the direct brine release calculation and corresponds to t_{int} in the solution of Eqs. (2) - (7) of Ref. 10, and R corresponds to the region in the computational grid for BRAGFLO that is mapped into the region in the computational grid for BRAGFLO_DBR that contains the point (*x*, *y*) (Fig. 2)

Values for $\phi(x, y, 0)$		
$\phi(x, y, 0) = 1 - h_i(1 - \phi_{WP,i}) / h(t_{int})$		(*x*, *y*) in waste panel in Fig. 1
$= h_{DRZ,i}\, \phi_{DRZ,i} / h(t_{int})$		(*x*, *y*) in DRZ in Fig. 1
$= h_{PS,i}\, \phi_{PS,i} / h(t_{int})$		(*x*, *y*) in panel seal in Fig. 1
$= h_{H,i}\, \phi_{H,i} / h(t_{int})$		(*x*, *y*) in undisturbed halite in Fig. 1

where h_i is initial height of waste panels (3.96 m), $\phi_{WP,i}$ is initial porosity of waste panels (0.848), $h(t_{int})$ is height of repository at time of intrusion (typically 1 to 1.5 m; corresponds to h in Eq. (5)), $h_{DRZ,i}$ is initial height for DRZ that results in DRZ in Fig. 1 having the same pore volume as the initial pore volume of the DRZ in Fig. 1 of Ref. 10 (8.98 m), $\phi_{DRZ,i}$ is initial porosity of DRZ (0.0129) (Note: $h_{DRZ,i}\, A_{DRZ}\, \phi_{DRZ,i}$ is equal to pore volume of DRZ in Fig. 1 of Ref. 10, where A_{DRZ} is area associated with DRZ in Fig. 1), $h_{PS,i}$ is initial height of panel seals (3.96 m), $\phi_{PS,i}$ is initial porosity of panel seals (0.075) (Note: $h_{PS,i}\, A_{PS}\, \phi_{PS,i}$ is equal to pore volume of panel seals in Fig. 1 of Ref. 10, where A_{PS} is area associated with panel seals in Fig. 1), $h_{H,i}$ is initial height of undisturbed halite in Fig. 1 (arbitrarily taken to be same as $h_{DRZ,i}$, which is 8.98 m), and $\phi_{H,i}$ is initial porosity of halite (0.01) (Note: due to its low permeability (3.16×10^{-23} m^2), undisturbed halite has little effect on results calculated over a short time period with the computational grid in Fig. 1 and so no effort was made to preserve halite pore volume when mapping from the computational grid in Fig. 1 of Ref. 10 to the computational grid in Fig. 1).

Table 2. Boundary Value Conditions for p_b and S_g in Solution of Eqs. (15) - (20) with Computational Grid in Fig. 1

(x, y) on Upper (Northern) or Lower (Southern) Boundary in Fig. 1, $0 \le t$
$\partial p_b\,(x, y, t)/\partial y = 0$ Pa/m, $\partial S_g\,(x, y, t)/\partial y = 0$ m^{-1}
(x, y) on Right (Eastern) or Left (Western) Boundary in Fig. 1, $0 \le t$
$\partial p_b\,(x, y, t)/\partial x = 0$ Pa/m, $\partial S_g\,(x, y, t)/\partial x = 0$ m^{-1}
(x, y) at Location of Drilling Intrusion under Consideration (see indicated points in Fig. 1), $0 \le t$
$p_b\,(x, y, t) = p_{wf}$ (see Sect. 5)
(x, y) at Location of Prior Drilling Intrusion that Penetrated Pressurized Brine (see indicated point in Fig. 1), $0 \le t$
$p_b\,(x, y, t) = p_{wE1}$ (see Sect. 6)

Table 3. Results Available for Use in CCDF Construction for Direct Brine Releases

$C_{E0}(\tau_k)$	=	concentration (EPA units/m^3) in brine in the repository under undisturbed conditions at time τ_k, where τ_k, k = 1, 2, ..., 9, corresponds to 100, 125, 175, 350, 1000, 3000, 5000, 7500 and 10,000 yr. Based on solubilities (*WSOLAM3S*, *WSOLPU3S*, *WSOLPU4S*, *WSOLU4S*, *WSOLU6S*, *WSOLTH4S*) and chemical conditions (*WOXSTAT*) for repository dominated by Salado brine; see Table 1, Ref. 12, and Fig. 14a. Source: PANEL
$C_{E1}(\tau_k)$	=	concentration (EPA units/m^3) in brine in the repository subsequent to an E1 intrusion at time τ_k, where τ_k, k = 1, 2, ..., 9, corresponds to 100, 125, 175, 350, 1000, 3000, 5000, 7500 and 10,000 yr. Based on solubilities (*WSOLAM3C*, *WSOLPU3C*, *WSOLPU4C*, *WSOLU6C*) and chemical conditions (*WPHUMOX3*, *WOXSTAT*) for repository dominated by Castile brine; see Table 1, Ref. 12, and Fig. 14b. Source: PANEL
$VB_{E0,U}(\tau_k)$	=	volume (m^3) of brine released by a drilling intrusion into a previously unintruded repository at time τ_k that encounters CH-TRU waste in an upper waste panel, where τ_k, k = 1, 2, ..., 6, corresponds to 100, 350, 1000, 3000, 5000 and 10,000 yr, respectively. See Fig. 7. Source: BRAGFLO_DBR.
$VB_{E0,L}(\tau_k)$	=	Same as $VB_{E0,U}(\tau_k)$ but for intrusion into a lower waste panel. See Fig. 7.
$VB_{E1,S}(\tau_j, \Delta\tau_{jk})$	=	volume (m^3) of brine released by second drilling intrusion at time $\tau_j + \Delta\tau_{jk}$ into the same waste panel penetrated by an initial E1 intrusion at time τ_j, where (1) τ_j, j = 1, 2, corresponds to 350 and 1000 yr, (2) $\tau_1 + \Delta\tau_{1k}$, k = 1, 2, ..., 7, corresponds to 350, 550, 750, 2000, 4000, 10,000 and 10,250 yr (i.e., $\Delta\tau_{1k}$ = 0, 200, 400, 1650, 3650, 9650, 9900 yr), results for k = 2, 3, ..., 6 are summarized in Fig. 10.1.6 of Ref. 20, $VB_{E1,S}(\tau_1, \Delta\tau_{11}) = VB_{E1,S}(\tau_1, \Delta\tau_{12})$ (i.e., $VB_{E1,S}$ (350,0) = $VB_{E1,S}$ (350, 200)), and $VB_{E1,S}(\tau_1, \Delta\tau_{16}) = VB_{E1,S}(\tau_1, \Delta\tau_{17})$ (i.e., $VB_{E1,S}$(350, 9650) = $VB_{E1,S}$(350, 9900), and (3) $\tau_2 + \Delta\tau_{2k}$, k = 1, 2, ..., 6, corresponds to 1000, 1200, 1400, 3000, 5000 and 10,000 yr (i.e., $\Delta\tau_{2k}$ = 0, 200, 400, 1000, 4000, 9000 yr), results for k = 2, 3, ..., 6 are summarized in Fig. 12a, and $VB_{E1,S}(\tau_1, \Delta\tau_{21}) = VB_{E1,S}(\tau_1, \Delta\tau_{22})$ (i.e., $VB_{E1,S}$ (1000, 0) = $VB_{E1,S}$ (1000, 200)). Source: BRAGFLO_DBR. The assignments $VB_{E1,S}$(350, 0) = $VB_{E1,S}$(350, 200) and $VB_{E1,S}$(1000, 0) = $VB_{E1,S}$(1000, 200) are made to bracket the time period between the occurrence of the first drilling intrusion and the failure of the plug at the Rustler/Salado interface; the assignment $VB_{E1,S}$ (350, 9650) = $VB_{E1,S}$ (350, 9900) is made to facilitate the use of $VB_{E1,S}(\tau_1, \Delta\tau_{1k})$ for initial intrusions before τ_1 = 350 yr.
$VB_{E1,D}(\tau_j, \Delta\tau_{jk})$	=	same as $VB_{E1,S}(\tau_j, \Delta\tau_{jk})$ but for intrusion into different waste panel. See Fig. 12a and Fig. 10.1.6 in Ref. 20.
$VB_{E2,S}(\tau_j, \Delta\tau_{jk})$	=	same as $VB_{E1,S}(\tau_j, \Delta\tau_{jk})$ but for initial E2 intrusion. See Fig. 12c and Fig. 10.1.7 in Ref. 20.
$VB_{E2,D}(\tau_j, \Delta\tau_{jk})$	=	same as $VB_{E1,D}(\tau_j, \Delta\tau_{jk})$ but for initial E2 intrusion. See Fig. 12c and Fig. 10.1.7 in Ref. 20.

Table 4. Determination of Direct Brine Release $f_{DB}(\mathbf{x}_{st})$ for an Arbitrary Future $\mathbf{x}_{st}$ of Form in Eq. (30) of Ref. 11

Release rDB_i for intrusion into nonexcavated area at time t_i: $rDB_i = 0$

Release rDB_i for intrusion into pressurized repository at time t_i (i.e., $i = 1$ or $\tilde{b}_j = 0$[a] for $j = 1, 2, \ldots, i-1$):

rDB_i	= 0	if intrusion penetrates RH-TRU waste
	= $C_{E0}(t_i)$[b] $VB_{E0,U}(t_i)$	if l_i in upper waste panel
	= $C_{E0}(t_i)$ $VB_{E0,L}(t_i)$	if l_i in upper waste panel.

Release rDB_i for intrusion into a depressurized repository at time t_i with no E1 intrusion in first $i - 1$ intrusions (i.e., $\tilde{b}_k = 0$ for $k = 1, 2, \ldots, j-1$, $\tilde{b}_j = 2$, $\tilde{b}_k \neq 1$ for $k = j+1, j+2, \ldots, i-1$):

rDB_i	= 0	if intrusion penetrates RH-TRU waste
	= $C_{E0}(t_i)$ $VB_{E2,S}(t_j, t_i - t_j)$[c]	if l_j, l_i in same waste panel
	= $C_{E0}(t_i)$ $VB_{E2,D}(t_j, t_i - t_j)$	if l_j, l_i in different waste panels.

Release rDB_i for intrusion into a depressurized repository at time t_i with first E1 intrusion at time $t_j < t_i$ (i.e., $\tilde{b}_k \neq 1$ for $k = 1, 2, \ldots, j-1$, $\tilde{b}_j = 1$):

rDB_i	= 0	if intrusion penetrates RH-TRU waste
	= $C_{E1}(t_i)$ $VB_{E1,S}(t_j, t_i - t_j)$	if l_j, l_i in same waste panel
	= $C_{E1}(t_i)$ $VB_{E1,D}(t_j, t_i - t_j)$	if l_j, l_i in different waste panels.

Spallings release $f_{BL}(\mathbf{x}_{st})$:

$$f_{DB}(\mathbf{x}_{st}) = \sum_{i=1}^{n} rDB_i$$

---

[a] See Table 3 in Ref. 11 for definition of $\tilde{b}_j = 0, 1, 2$.

[b] Here and elsewhere, appearance of an undefined time implies linear interpolation between defined times in Table 3.

[c] Here and elsewhere, appearance of two undefined times implies two-dimensional linear interpolation between defined times in Table 3.

Table 5. Stepwise Regression Analyses with Rank-Transformed Data for Expected Volume and Expected Normalized Release Associated with Individual CCDFs for Direct Brine Release

	Expected Volume			Expected Normalized Release		
Step[a]	Variable[b]	SRRC[c]	R^{2d}	Variable	SRRC	R^2
1	*WRBRNSAT*	−0.44	0.19	*WRBRNSAT*	−0.46	0.21
2	*HALPOR*	0.35	0.32	*HALPOR*	0.37	0.35
3	*ANHPRM*	0.28	0.39	*ANHPRM*	0.27	0.42
4	*BPCOMP*	0.22	0.44	*BPCOMP*	0.20	0.46
5	*HALPRM*	0.15	0.46	*BPINTPRS*	0.14	0.48
6	*BPINTPRS*	0.14	0.48	*HALPRM*	0.14	0.50
7	*BPVOL*	0.11	0.49			

[a] Steps in stepwise regression analysis.

[b] Variables listed in order of selection in regression analysis with *ANHCOMP* and *HALCOMP* excluded from entry into regression model due to −0.99 rank correlations imposed on the variable pairs (*ANHPRM, ANHCOMP*) and (*HALPRM, HALCOMP*) (see Sect. 7.2, Ref. 20).

[c] Standardized rank regression coefficients in final regression model.

[d] Cumulative R^2 value with entry of each variable into regression model.

Table 6. Solubilities Used in Sensitivity Studies Associated with Releases from the Repository (see Table 1 of Ref. 12 for definitions of individual solubilities)

Variable	Definition
SOLAMC	Solubility (mol/1) of americium in Castile brine.
SOLPUC	Solubility (mol/1) of plutonium in Castile brine.
SOLTHC	Solubility (mol/1) of thorium in Castile brine.
SOLUC	Solubility (mol/1) of uranium in Castile brine.
SOLAMS	Solubility (mol/1) of americium in Salado brine.
SOLPUS	Solubility (mol/1) of plutonium in Salado brine.
SOLTHS	Solubility (mol/1) of thorium in Salado brine.
SOLUS	Solubility (mol/1) of uranium in Salado brine.